Non-associative J2 plasticity model for finite element buckling analysis of shells in the inelastic range

NON-ASSOCIATIVE J_2 PLASTICITY MODEL FOR FINITE ELEMENT BUCKLING ANALYSIS OF SHELLS IN THE INELASTIC RANGE

Patricia Pappa, Spyros A. Karamanos[i]
Department of Mechanical Engineering
University of Thessaly
Volos, GR-38334, Greece

Keywords: Plasticity, Constitutive model, Finite element, Buckling, Shells, Structural stability.

Abstract. *The development and numerical implementation of a special-purpose constitutive model is described for investigating the structural stability of cylindrical metal shells under axial compression and bending, which buckle in the inelastic range. The model employs von Mises yield surface (J_2 plasticity) and the rate form of J_2 deformation theory, leading to a non-associated flow rule. Special emphasis is given on plastic flow continuity. The numerical implementation is conducted through both the classical Euler-backward and Euler-forward substitution numerical schemes, where stress and strain tensors are described in curvilinear coordinates, with the extra constraint of zero normal stress through the shell thickness. The numerical results will be compared with available experimental data. The model is implemented within an in-house finite element technique for the nonlinear analysis of relatively thick cylindrical metal shells that uses a "tube-element" discretization, and it is employed for the solution of some benchmark problems.*

1 INTRODUCTION

Relatively thick cylindrical metal shells, with diameter-to-thickness ratio $D/t_s \le 50$, are used in pipeline and piping applications for hydrocarbon transportation and distribution. Those elongated metal cylinders, often referred to as "tubes" or "pipes", can be subjected to severe structural loading, which induces significant compressive strains in the cylinder wall, resulting in buckling failure in the form of wrinkles, sometimes referred to as "local buckling". This is a shell-type buckling, quite different from the one that thin-walled shells exhibit. More specifically, thin-walled cylindrical shells under axial compression buckle in the elastic range, and their behavior is characterized by sudden collapse and imperfection sensitivity. On the contrary, thick-walled cylinders buckle in the plastic range and failure occurs more gradually after a sequence of events.

Early experimental work has been reported on relatively-thick aluminum cylinders by Lee (1962) and Batterman (1965), supported by analytical bifurcation calculations, demonstrated that the buckling resistance of relatively-thick metal cylindrical shells is less sensitive to initial imperfections than of thin-walled elastic shells. The imperfection sensitivity of axially compressed cylindrical shells has been investigated analytically by Gellin (1979), extending Koiter's methodology for cylindrical shells considering a uniform axisymmetric imperfection (Koiter, 1963). A recent experimental and analytical investigation of buckling behavior of thick cylindrical shells has been reported by Bardi and Kyriakides (2006) and Bardi et al. (2006), whereas local buckling of elongated cylindrical shells under longitudinal bending has been examined in the works of Kyriakides and Ju (1992), and Ju

[i] corresponding author. Tel +30 24210 74086, FAX +30 24210 74012, email: skara@mie,uth.gr.

and Kyriakides (1992).

In simulating metal shell buckling in the inelastic range, the choice of appropriate material models constitutes a key issue. It has been recognized that J_2-flow theory can accurately describe the general material behavior of metals in the inelastic range and it is widely used for the nonlinear elastic-plastic finite element stress analysis of shell structures (Dvorkin et al., 1995, Argyris et al., 2002, Paraskevopoulos and Talaslidis, 2006). Nevertheless, buckling predictions based on the J_2-flow theory may not be reliable in cases where bifurcation from the prebuckling state occurs well into the inelastic range. This is attributed to the vertex (corner) that develops on the yield surface at the point of loading. The formation of such vertex on the yield surface has been detected experimentally in aluminum and steel materials (Kuwabara et al., 2000), and can be very important in cases, where abrupt deviations from proportional loading occur, as in the case of plastic instability, where the shell wall exhibits a transition from a smooth configuration to a wavy-pattern associated with multi-axial state of stress.

To obtain more reliable buckling predictions, in axially-compressed cylindrical metal shells Tvergaard (1983) and Mikkelsen (1995) conducted stability calculations through a special enhancement of J_2 (von Mises) plasticity theory, namely the J_2-corner theory, initially proposed by Christoffersen and Hutchinson (1979), considering the formation of a corner on the yield surface at the loading point. Using J_2-corner theory, the corresponding instantaneous moduli are less stiff than those predicted by the J_2-flow theory. Therefore, the response is significantly different for the case of abrupt change of direction in the stress space (e.g. when buckling occurs), while for proportional loading the two theories coincide. Nevertheless, the corner theory, despite its rigorousness in describing the corner of the yield surface, may not be suitable for large-scale computations.

Alternatively, pseudo-corner theories have been proposed. Hughes and Shakib (1986) presented a modified J_2-flow theory with a hardening modulus that depends on the angle between the deviatoric strain increment and the outward vector normal to the yield surface. In this simplistic manner, the model attempts to account for some essential characteristic of a corner theory, such as reduced material stiffness and increased plastic flow, while keeping the basic features of the classical J_2-flow theory. Simo (1987) proposed a J_2-non-associative flow model, which imitates some corner theory characteristics through the adoption of a non-associative flow rule without introducing the complexity associated with keeping track of the formation and evolution of yield surface corners. Simo also presented an Euler-backward scheme for the numerical integration of the pseudo-corner model within a non-linear finite element framework. However, Simo's pseudo-corner model requires the definition of several parameters related to the yield surface "vertex". In addition it is not clear how the proposed integration scheme can be implemented in shell analysis problems. This model has not been used in large-scale inelastic shell buckling calculations.

So far, most of the attempts to predict bifurcation buckling in the inelastic range use the flow theory for tracing the prebuckling solution and employ the deformation theory moduli to detect bifurcation on the prebuckling path (e.g. Ju and Kyriakides, 1992, Bardi et al., 2006). However, such an approach does not describe accurately the entire structural response, and most importantly, postbuckling performance. In a more recent publication, Peek (2000) developed a J_2 plasticity model, which uses a non-associated flow rule similar to the rate form of the J_2 deformation theory referred to as "incrementally continuous" deformation theory with unloading and the proposed constitutive model can be implemented with minimal changes to an algorithm based on associative flow theory. This model is an important contribution towards elastic-plastic buckling analysis, however its main drawback is that in this model unloading is not elastic. Furthermore, its implementation to shell buckling problems, where zero

normal stress should be zero through shell thickness, is not described.

The present paper describes the development and the numerical implementation of an efficient special-purpose constitutive model, suitable for accurate and efficient large-scale metal shell buckling computations within a finite element environment. The material model is based on the von Mises yield surface (J_2 plasticity) with isotropic hardening and employs the rate form of J_2-deformation theory, leading to a non-associated flow rule. The numerical implementation follows an Euler-backward or an Euler-forward substitution scheme, developed for elastic-plastic shell analysis, accounting for zero normal stress through the shell thickness. The model maintains the basic features of the classical J_2-flow plasticity implementation, while introducing the key enhancements for accurate and efficient shell buckling predictions. Furthermore an enhanced version of the model is developed, which allows the simple and efficient extension of the model for large strains through an additive decomposition of the rate-of-deformation tensor.

The proposed constitutive model and its numerical integration are presented in the framework of small-strain plasticity in section 2, whereas section 3 describes the direct enhancement of the model for large strains. The non-associative constitutive model is incorporated in a special-purpose finite element methodology, outlined in section 4; the methodology has been introduced elsewhere for the analysis of nonlinear cylindrical shells, and has been shown very efficient for analyzing the structural behavior of steel cylinders (Karamanos and Tassoulas 1996). In section 5, the issue of plastic flow continuity is addressed, whereas in section 6 three characteristic problems are modeled and the numerical results are compared with existing analytical results and available experimental data.

2 CONSTITUTIVE MODEL

In this section, a description of the model for small-strain analysis is presented, followed by its numerical integration and the development of the consistent elastic rigidity matrix.

2.1 Model description

The rate of stress $\dot{\boldsymbol{\sigma}}$ is related to the elastic strain rate $\dot{\boldsymbol{\varepsilon}}^e$ as follows:

$$\dot{\boldsymbol{\sigma}} = \mathbf{D}\dot{\boldsymbol{\varepsilon}}^e = \mathbf{D}\left(\dot{\boldsymbol{\varepsilon}} - \dot{\boldsymbol{\varepsilon}}^p\right) \tag{1}$$

where $\mathbf{D}$ is the fourth order elastic stiffness tensor, $\dot{\boldsymbol{\varepsilon}}$ is the rate of total strain and $\dot{\boldsymbol{\varepsilon}}^p$ is the plastic strain rate. The elastic rigidity $\mathbf{D}$ can be expressed as follows:

$$\mathbf{D} = 2G\,\mathbf{I} + 3\left(K - \frac{2}{3}G\right)\mathbf{J} \tag{2}$$

where K is the bulk modulus, G is the shear modulus, $\mathbf{I}$ is the symmetric fourth-order identity tensor and $\mathbf{J}$ is the volumetric fourth-order identity tensor. Tensor $\mathbf{D}$ can also be written in the following form:

$$\mathbf{D} = 2G\,\mathbf{P} + 3K\,\mathbf{J} \tag{3}$$

where the fourth-order tensor $\mathbf{P}$ is defined as

$$\mathbf{P} = \mathbf{I} - \mathbf{J} \tag{4}$$

In the present model, the flow rule adopts the rate form of the J_2-deformation theory:

$$\dot{\boldsymbol{\varepsilon}}^p = \frac{3}{2}\left(\frac{1}{E_s} - \frac{1}{E}\right)\dot{\mathbf{s}} + \frac{3}{2}\frac{\dot{q}}{q}\left(\frac{1}{E_T} - \frac{1}{E_s}\right)\mathbf{s} \tag{5}$$

where $\mathbf{s}$ is the deviatoric stress tensor, q is the von Mises equivalent stress, defined as follows

$$q = \sqrt{\frac{3}{2}\mathbf{s}\cdot\mathbf{s}} = \sqrt{3J_2} \tag{6}$$

so that

$$\dot{q} = \frac{3}{2q}\mathbf{s}\cdot\dot{\mathbf{s}} \tag{7}$$

and E, E_s, E_T are the Young's modulus, the secant modulus and the tangent modulus respectively. Yielding is defined is defined by the von Mises yield function with isotropic hardening

$$F\left(\boldsymbol{\sigma}, \varepsilon_q\right) = \frac{1}{2}\mathbf{s}\cdot\mathbf{s} - \frac{1}{3}k^2\left(\varepsilon_q\right) = 0 \tag{8}$$

where $k = k\left(\varepsilon_q\right)$ is the material yield stress in uniaxial tension, which defines the size of the yield surface, ε_q is the equivalent plastic strain, defined as follows

$$\dot{\varepsilon}_q = \sqrt{2/3}\ \dot{\boldsymbol{\varepsilon}}^p \cdot \mathbf{n} \tag{9}$$

and $\mathbf{n} = \mathbf{s}/\|\mathbf{s}\|$ is the unit outward normal tensor to the yield surface and $\|\mathbf{s}\|$ is the magnitude of $\mathbf{s}$ ($\|\mathbf{s}\| = \sqrt{\mathbf{s}\cdot\mathbf{s}}$). Function $k\left(\varepsilon_q\right)$ can be nonlinear, and is calibrated from a uniaxial tension test.

The plastic strain rate equation (5) can be rewritten in the following, more illustrative vector form

$$\dot{\boldsymbol{\varepsilon}}^p = \frac{3\dot{\varepsilon}_q}{2q}\mathbf{s} + \frac{3}{2}\left(\frac{1}{E_s} - \frac{1}{E}\right)\dot{\mathbf{s}}^t \tag{10}$$

where $\dot{\mathbf{s}}^t = \dot{\mathbf{s}} - \left(\mathbf{n}\cdot\dot{\mathbf{s}}\right)\mathbf{n}$ is the component of $\dot{\mathbf{s}}$ tangent to the yield surface shown in Figure 1. The flow rule in equation (10) implies that the plastic strain increment is composed by two components, one normal to the yield surface and one tangent to the yield surface. This makes the elastic-plastic instantaneous moduli of the J_2-deformation less stiff than the corresponding moduli of the J_2-flow theory. More specifically, the instantaneous rigidity tensor (tangent moduli) for this model can be written as follows

$$\mathbf{D}_{ep} = 2G_s\mathbf{I} + 3\left(K - \frac{2}{3}G_s\right)\mathbf{J} - \frac{3}{q^2}\left(G_s - G_T\right)\left(\mathbf{s}\otimes\mathbf{s}\right) \tag{11}$$

where

$$G_s = \frac{1}{\frac{1}{G} + \frac{3}{h}} \tag{12}$$

$$G_T = \frac{1}{\frac{1}{G} + \frac{3}{H}} \tag{13}$$

$$h = \frac{1}{\frac{1}{E_s} + \frac{1}{E}} \tag{14}$$

and H is the hardening modulus, equal to $dk/d\varepsilon_q$.

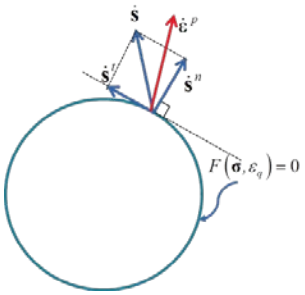

Figure 1: Schematic representation of stress and strain tensor increments in the deviatoric plane, with respect to von Mises surface.

A curvilinear system ξ^1, ξ^2,ξ^3 is considered to describe stress and deformation within the shell, where coordinate lines ξ^1 and ξ^2 for a constant value of ξ^3 define a shell surface (lamina), whereas the coordinate line ξ^3 is initially directed through the shell thickness. The covariant and contravariant base vectors of this coordinate system are denoted as $\mathbf{g}_i$ and $\mathbf{g}^j$ respectively, as shown in Figure 2. Therefore, the stress tensor can be written in terms of the covariant tensor base $\boldsymbol{\sigma} = \sigma^{ij}\left(\mathbf{g}_i \otimes \mathbf{g}_j\right)$, and the components of fourth-order rigidity tensors $\mathbf{D}$ and $\mathbf{D}_{ep}$ with respect to the covariant basis can be written

$$D^{ijkl} = G\left(g^{jl}g^{ik} + g^{il}g^{jk}\right) + \left(K - \frac{2}{3}G\right)g^{ij}g^{kl} \tag{15}$$

and

$$D_{ep}^{ijkl} = G_s\left(g^{jl}g^{ik} + g^{il}g^{jk}\right) + \left(K - \frac{2}{3}G_s\right)g^{ij}g^{kl} - \frac{3}{q^2}\left(G_s - G_T\right)s^{ij}\,s^{kl} \tag{16}$$

Finally, in the present formulation, following shell theory, it is required that the traction component normal to any shell lamina is imposed to be zero at any stage of deformation. Considering that the traction on the lamina is $\frac{1}{\left\|\mathbf{g}^3\right\|}\boldsymbol{\sigma}\mathbf{g}^3$, where $\left\|\mathbf{g}^3\right\|$ is the magnitude of $\mathbf{g}^3$, i.e. the contravariant base vector normal to the ξ^1, ξ^2-surface (as shown in Figure 2), and that traction component normal to the lamina is $\frac{1}{\left\|\mathbf{g}^3\right\|^2}\boldsymbol{\sigma}\cdot(\mathbf{g}^3 \otimes \mathbf{g}^3)$, which is equal to $\frac{1}{\left\|\mathbf{g}^3\right\|^2}\sigma^{33}$, one obtains

$$\sigma^{33} = 0 \tag{17}$$

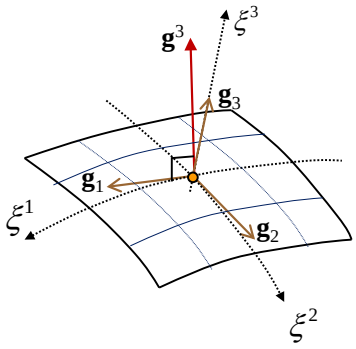

Figure 2: Curvilinear coordinate system and base vectors for shell description.

2.2 Numerical Implementation

Consider that at a material point, the stress $\boldsymbol{\sigma}_n$, strain $\boldsymbol{\varepsilon}_n$ and the equivalent plastic strain $\varepsilon_{q|n}$ are given at time t_n, as well as the strain $\boldsymbol{\varepsilon}_{n+1} = \boldsymbol{\varepsilon}_n + \Delta\boldsymbol{\varepsilon}$ at time t_{n+1}. The calculation of $\boldsymbol{\sigma}_{n+1}$ and $\varepsilon_{q|n+1}$ requires integration of the above constitutive equations from t_n to t_{n+1}. An elastic predictor – plastic corrector scheme is adopted where a purely elastic trial state is followed by a plastic corrector phase. The purely elastic (trial) stress is defined by the formula

$$\boldsymbol{\sigma}^e = \boldsymbol{\sigma}_n + \mathbf{D}\Delta\boldsymbol{\varepsilon} \tag{18}$$

In accordance with condition (17), the strain increment is decomposed as follows

$$\Delta\boldsymbol{\varepsilon} = \Delta\overline{\boldsymbol{\varepsilon}} + \Delta\varepsilon_{33}\left(\mathbf{g}^3 \otimes \mathbf{g}^3\right) \tag{19}$$

where $\Delta\overline{\boldsymbol{\varepsilon}}$ is the known part of the total strain increment $\Delta\boldsymbol{\varepsilon}$, and $\Delta\varepsilon_{33}$ is an extra unknown (Aravas, 1987).

If the trial stress violates the yield condition, an elastic-plastic behavior should be taken into account, integrating equation (1) between stages t_n and t_{n+1},

$$\boldsymbol{\sigma}_{n+1} = \boldsymbol{\sigma}_n + \mathbf{D}\left(\Delta\boldsymbol{\varepsilon} - \Delta\boldsymbol{\varepsilon}^p\right) \tag{20}$$

Using an Euler-backward integration scheme for equation (5), the increment of plastic strain is written

$$\Delta\boldsymbol{\varepsilon}^p = \frac{3}{2h_{n+1}}\left(\mathbf{s}_{n+1} - \mathbf{s}_n\right) + \frac{3}{2}\frac{\Delta\varepsilon_q H_{n+1}}{q_{n+1}h_{1|n+1}}\mathbf{s}_{n+1} \tag{21}$$

where the von Mises equivalent final stress is

$$q_{n+1} = \sqrt{3\mathbf{s}_{n+1}\cdot\mathbf{s}_{n+1}/2} \tag{22}$$

and

$$h_1 = \left(1/E_T - 1/E_s\right) \tag{23}$$

Using eqs. (19) and (21), the final stress becomes

$$\boldsymbol{\sigma}_{n+1} = \overline{\boldsymbol{\sigma}}^e + 2G\,\Delta\varepsilon_{33}\mathbf{a} - \frac{3G}{h_{n+1}}\left(\mathbf{s}_{n+1} - \mathbf{s}_n\right) - \frac{3G\,\Delta\varepsilon_q H_{n+1}}{q_{n+1}h_{1|n+1}}\mathbf{s}_{n+1} \tag{24}$$

where

$$\overline{\boldsymbol{\sigma}}^e = \boldsymbol{\sigma}_n + \mathbf{D}\Delta\overline{\boldsymbol{\varepsilon}} \tag{25}$$

$$\mathbf{a} = \mathbf{g}^3 \otimes \mathbf{g}^3 \tag{26}$$

and $\mathbf{a}'$ is the deviatoric part of $\mathbf{a}$. From equation (24), the hydrostatic and the deviatoric parts of the final stress are written as

$$p_{n+1} = \overline{p}^e - K\,\Delta\varepsilon_{33}\,g^{33} \tag{27}$$

$$\mathbf{s}_{n+1} = \frac{1}{1+\dfrac{3G}{h_{n+1}}+\dfrac{3G\,\Delta\varepsilon_q\,H_{n+1}}{q_{n+1}h_{1|n+1}}}\left(\overline{\mathbf{s}}^e + 2G\,\Delta\varepsilon_{33}\mathbf{a}' + \frac{3G}{h_{n+1}}\mathbf{s}_n\right) \tag{28}$$

where $\overline{p}^e\,\mathbf{1}$ and $\overline{\mathbf{s}}^e$ are the hydrostatic and deviatoric parts of $\overline{\boldsymbol{\sigma}}^e$ ($\overline{\boldsymbol{\sigma}}^e = -\overline{p}^e\,\mathbf{1} + \overline{\mathbf{s}}^e$). Equation (28) shows that $\mathbf{s}_{n+1}$ and $\overline{\mathbf{s}}^e$ may not be co-linear and the correction may not be on the deviatoric plane. Squaring equation (28), the effective stress at the final state is calculated as follows

$$\begin{aligned} q_{n+1} = \frac{1}{1+\dfrac{3G}{h_{n+1}}}\Bigg\{\Bigg(\left(\overline{q}^{\mathrm{e}}\right)^2 + \left(\frac{3G}{h_{n+1}}q_n\right)^2 + \frac{6G}{h_{n+1}}Q^2 + 4G^2\,\Delta\varepsilon_{33}^2\,g^{33}\,g^{33} + \\ +6G\,\Delta\varepsilon_{33}\left(\overline{s}^{(e)^{33}} + \frac{3G}{h_{n+1}}s_n^{33}\right)\Bigg)^{1/2} - \frac{3G\,H_{n+1}}{h_{1|n+1}}\Delta\varepsilon_q\Bigg\} \end{aligned} \tag{29}$$

where

$$\overline{q}^e = \sqrt{(3/2)\,\overline{\mathbf{s}}^e \cdot \overline{\mathbf{s}}^e} \tag{30}$$

and

$$Q = \sqrt{(3/2)\,\overline{\mathbf{s}}^e \cdot \mathbf{s}_n} \tag{31}$$

The yield criterion (8) at stage $n+1$ is written as

$$q_{n+1}\left(\Delta\varepsilon_q, \Delta\varepsilon_{33}\right) = k\left(\varepsilon_q\big|_n + \Delta\varepsilon_q\right) \tag{32}$$

Enforcing the conditions of zero stress normal to any shell lamina ($\sigma_{n+1}^{33} = 0$), and using (24) the following equation is obtained

$$\left(1+\frac{3G}{h_{n+1}}+\frac{3G\,\Delta\varepsilon_q\,H_{n+1}}{q_{n+1}h_{1|n+1}}\right)p_{n+1}\,g^{33} - \left(\overline{s}^{(e)^{33}} + \frac{4G}{3}\Delta\varepsilon_{33}\,g^{33}\,g^{33} + \frac{3G}{h_{n+1}}s^{33}\right) = 0 \tag{33}$$

Summarizing, equations (27), (29), (33) and the yield criterion (32), constitute a system of four equations with four unknowns, namely, q_{n+1}, p_{n+1}, $\Delta\varepsilon_q$ and $\Delta\varepsilon_{33}$. Considering $\Delta\varepsilon_q$ and $\Delta\varepsilon_{33}$ as the primary unknowns, equations (33) and (32), can be solved in terms of $\Delta\varepsilon_q$, $\Delta\varepsilon_{33}$ using Newton's method as described in more detail in Appendix I.

Alternatively, an Euler-forward method can be employed to integrate the above constitutive equations, within an elastic predictor–plastic corrector scheme. The Euler-forward integration of plastic strain rate gives

$$\Delta\boldsymbol{\varepsilon}^p = \frac{3}{2h_n}\left(\mathbf{s}_{n+1} - \mathbf{s}_n\right) + \frac{3}{2}\frac{\dot{\varepsilon}_q\,H_n}{q_n\,h_{1|n}}\mathbf{s}_n \tag{34}$$

The final stress and its deviatoric part are written as

$$\boldsymbol{\sigma}_{n+1} = \overline{\boldsymbol{\sigma}}^{e} + 2G\,\Delta\varepsilon_{33}\mathbf{a} - \frac{3G}{h_n}\left(\mathbf{s}_{n+1} - \mathbf{s}_n\right) - \frac{3G\,\Delta\varepsilon_q\,H_n}{q_n h_{1|n}}\mathbf{s}_n \tag{35}$$

$$\mathbf{s}_{n+1} = \frac{1}{1+\dfrac{3G}{h_n}}\left(\overline{\mathbf{s}}^{e} + 2G\,\Delta\varepsilon_{33}\mathbf{a}' + \left(\frac{3G}{h_n} - \frac{3G\,H_n}{q_n\,h_{1|n}}\Delta\varepsilon_q\right)\mathbf{s}_n\right) \tag{36}$$

Squaring equation (36), the effective stress at the final state is calculated as follows

$$\begin{aligned} q_{n+1} = \frac{1}{\left(1+\dfrac{3G}{h_n}\right)}\Bigg\{ & \left(\overline{q}^{e}\right)^2 + \left(\frac{3G}{h_n} - \frac{3GH}{q_n h_{1|n}}\Delta\varepsilon_q\right)^2 \left(q_n\right)^2 + \left(\frac{6G}{h_n} - \frac{6GH_n}{q_n h_{1|n}}\Delta\varepsilon_{\mathrm{q}}\right)(Q)^2 \\ & + 4G^2\,\Delta\varepsilon_{33}^2\,g^{33}\,g^{33} + 6G\,\Delta\varepsilon_{33}\left(\overline{s}^{(e)^{33}} + \left(\frac{3G}{h_n} - \frac{3GH}{q_n h_{1|n}}\Delta\varepsilon_q\right)s_n^{33}\right)\Bigg\}^{1/2} \end{aligned} \tag{37}$$

In addition, enforcing $\sigma_{n+1}^{33} = 0$ in equation (35), the following equation is obtained

$$\left(1+\frac{3G}{h_n}\right)p_{n+1}\,g^{33} - \left(\overline{s}^{(e)^{33}} + \frac{4}{3}G\,\Delta\varepsilon_{33}\,g^{33}\,g^{33} + \left(\frac{3G}{h_n} - \frac{3G\,\Delta\varepsilon_q\,H}{q_n h_{1|n}}\right)s_n^{33}\right) = 0 \tag{38}$$

Equations (27), (37), (38) and the yield criterion (32) constitute a system of four equations with four unknowns, namely, q_{n+1}, p_{n+1}, $\Delta\varepsilon_q$ and $\Delta\varepsilon_{33}$. Considering $\Delta\varepsilon_q$ and $\Delta\varepsilon_{33}$ as the primary unknowns, equations (38) and (32) can be solved in terms of $\Delta\varepsilon_q$, $\Delta\varepsilon_{33}$ using Newton's method as described in more detail in Appendix I.

2.3 Linearization moduli

The consistent (algorithmic) rigidity moduli are computed from the following basic equation:

$$\mathbf{D}_{ep}^{c} = \frac{\partial\boldsymbol{\sigma}_{n+1}}{\partial\boldsymbol{\varepsilon}_{n+1}} \tag{39}$$

The final stress is written in terms of its deviatoric part

$$\boldsymbol{\sigma}_{n+1} = \mathbf{s}_{n+1} + K\left(\boldsymbol{\varepsilon}_{n+1}\cdot\mathbf{1}\right)\mathbf{1} \tag{40}$$

where $\mathbf{1}$ is the second-order unit tensor, and the final strain

$$\boldsymbol{\varepsilon}_{n+1} = \mathbf{e}_{n+1} + \frac{1}{3}\left(\boldsymbol{\varepsilon}_{n+1}\cdot\mathbf{1}\right)\mathbf{1} \tag{41}$$

where $\mathbf{e}$ is the deviatoric strain tensor. Differentiation of equation (41) gives

$$\frac{\partial\mathbf{e}_{n+1}}{\partial\boldsymbol{\varepsilon}_{n+1}} = \mathbf{P} \tag{42}$$

Equation (39), with the consideration of equations (40) and (42), leads to

$$\mathbf{D}_{ep}^{c} = \frac{\partial\boldsymbol{\sigma}_{n+1}}{\partial\boldsymbol{\varepsilon}_{n+1}} = \frac{\partial\mathbf{s}_{n+1}}{\partial\mathbf{e}_{n+1}}\mathbf{P} + 3K\,\mathbf{I} \tag{43}$$

In the following, four-order tensor $\partial\boldsymbol{\sigma}_{n+1}/\partial\boldsymbol{\varepsilon}_{n+1}$ is computed for the Euler-backward integration scheme and

presented in the previous section. In particular using equations (18), (19) and (21), the final stress $\boldsymbol{\sigma}_{n+1}$ can be written as

$$\boldsymbol{\sigma}_{n+1} = \boldsymbol{\sigma}^e - 2G\left\{\frac{3}{2h_{n+1}}\left(\mathbf{s}_{n+1}-\mathbf{s}_n\right)+\frac{H\,\Delta\varepsilon_q}{h_{1|n+1}}\mathbf{N}_{n+1}\right\} \tag{44}$$

where the dimensionless tensor $\mathbf{N}$ is defined at a certain stress state $\boldsymbol{\sigma}$ by the following expression:

$$\mathbf{N} = \frac{3}{2q}\mathbf{s} \tag{45}$$

Using the definition of the equivalent stress in equation (6), it can be readily verified that

$$\frac{\partial q}{\partial \boldsymbol{\sigma}} = \mathbf{N} \tag{46}$$

The corresponding deviatoric stress is

$$\mathbf{s}_{n+1} = \mathbf{s}^e - 2G\left\{\frac{3}{2h_{n+1}}\left(\mathbf{s}_{n+1}-\mathbf{s}_n\right)+\frac{H\,\Delta\varepsilon_q}{h_{1|n+1}}\mathbf{N}_{n+1}\right\} \tag{47}$$

or equivalently,

$$\mathbf{s}_{n+1} = \frac{1}{1+\dfrac{3G}{h_{n+1}}+\dfrac{3G\,H\,\Delta\varepsilon_q}{q_{n+1}\,h_{1|n+1}}}\left(\mathbf{s}^e+\frac{3G}{h_{n+1}}\mathbf{s}_n\right) \tag{48}$$

Differentiation of equation (47) gives

$$d\,\mathbf{s}_{n+1} = d\,\mathbf{s}^e - 3G\,d\left(\frac{\mathbf{s}_{n+1}}{h_{n+1}}\right)-3G\,d\left(\frac{H\,\Delta\varepsilon_q}{q_{n+1}\,h_{1|n+1}}\mathbf{s}_{n+1}\right)+3G\,\mathbf{s}_n\,d\left(\frac{1}{h_{n+1}}\right) \tag{49}$$

From the definition of the trial stress in equation (18), it is readlily obtained that

$$d\,\mathbf{s}^e = 2G\,d\,\mathbf{e}_{n+1} = 2G\,\mathbf{P}\,d\,\boldsymbol{\varepsilon}_{n+1} \tag{50}$$

Furthermore, it is necessary to express differential quantities $d\,\varepsilon_q$, $d\,\mathbf{s}_{n+1}$ and dq_{n+1} in terms of $d\,\boldsymbol{\varepsilon}_{n+1}$. Squaring equation (48) and assuming that tensor $\mathbf{s}^e$ is parallel to $\mathbf{s}_n$, the von Mises equivalent stress at the final state is calculated as follows

$$q_{n+1} = \frac{1}{1+\dfrac{3G}{h_{n+1}}}\left(q^e+\frac{3G}{h_{n+1}}q_n-\frac{3G\,H_{n+1}}{h_{1|n+1}}\Delta\varepsilon_q\right) \tag{51}$$

where $q^e = \sqrt{(3/2)\mathbf{s}^e\cdot\mathbf{s}^e}$ and $q_n = \sqrt{(3/2)\mathbf{s}_n\cdot\mathbf{s}_n}$. The assumption of tensors $\mathbf{s}^e$ and $\mathbf{s}_n$ being co-axial is discussed at the end of the paragraph. From the definition of the hardening modulus,

$$d\,q_{n+1} = H_{n+1}\,d\,\varepsilon_q \tag{52}$$

The final stress has to satisfy the yield criterion and using equations (32) and (51) this can be expressed as follows

$$q^e+\frac{3G}{h_{n+1}}q_n-\frac{3G\,H_{n+1}}{h_{1|n+1}}\Delta\varepsilon_q = \left(1+\frac{3G}{h_{n+1}}\right)k\left(\varepsilon_{q|n}+\Delta\varepsilon_q\right) \tag{53}$$

Differentiation of equation (53) gives

$$\frac{3}{2q^e}\mathbf{s}^e\left(\mathbf{D}\,d\,\boldsymbol{\varepsilon}_{n+1}\right)+3G\,q_n\left(-\frac{h'_{n+1}}{h^2_{n+1}}\right)d\,\varepsilon_q-3G\,H_{n+1}\,\Delta\varepsilon_q\left(-\frac{h'_{1|n+1}}{h^2_{1|n+1}}\right)d\,\varepsilon_q$$
$$-\frac{3G\,\Delta\varepsilon_q\,H'_{n+1}}{h_{1|n+1}}d\,\varepsilon_q-\frac{3G\,H_{n+1}}{h_{1|n+1}}d\,\varepsilon_q=3G\,k\left(-\frac{h'_{n+1}}{h^2_{n+1}}\right)d\,\varepsilon_q+\left(1+\frac{3G}{h_{n+1}}\right)H_{n+1}\,d\,\varepsilon \tag{54}$$

or equivalently,

$$d\,\varepsilon_q=\frac{2G}{A}\mathbf{N}^e\,d\,\boldsymbol{\varepsilon}_{n+1} \tag{55}$$

where

$$A=\left(1+\frac{3G}{h_{n+1}}\right)H_{n+1}-\frac{3G\,q_{n+1}\,h'_{n+1}}{h^2_{n+1}}-\frac{3G\,H_{n+1}\,\Delta\varepsilon_q\,h'_{1|n+1}}{h^2_{1|n+1}}+\frac{3G\,\Delta\varepsilon_q\,H'_{n+1}}{h_{1|n+1}}+\frac{3G\,H_{n+1}}{h_{1|n+1}}+\frac{3G\,h'_{n+1}\,q_n}{h^2_{n+1}} \tag{56}$$

Subsequently, equations (50), (52) and (55) are substituted into (49)

$$d\,\mathbf{s}_{n+1}=\frac{2G}{B}\mathbf{P}\,d\,\boldsymbol{\varepsilon}_{n+1}-\frac{4G}{3}\left(\frac{1}{B}-\frac{H}{A}\right)\mathbf{N}\otimes\mathbf{N}\,d\,\boldsymbol{\varepsilon}_{n+1} \tag{57}$$

where

$$B=1+\frac{3G}{h_{n+1}}+\frac{3G\,H\,\Delta\varepsilon_q}{q_{n+1}\,h_{1|n+1}} \tag{58}$$

Substituting,

$$d\,\boldsymbol{\sigma}_{n+1}=\mathbf{D}\,d\,\boldsymbol{\varepsilon}_{n+1}-\frac{4G}{3}\left[\left(\frac{1}{B}-\frac{H}{A}\right)\mathbf{N}_{n+1}\otimes\mathbf{N}_{n+1}+\frac{3}{2}\left(1-\frac{1}{B}\right)\mathbf{P}\right]d\,\boldsymbol{\varepsilon}_{n+1} \tag{59}$$

so that the consistent rigidity tensor (algorithmic moduli)

$$\mathbf{D}^c_{ep}=\mathbf{D}-\frac{4G}{3}\left[\left(\frac{1}{B}-\frac{H}{A}\right)\mathbf{N}_{n+1}\otimes\mathbf{N}_{n+1}+\frac{3}{2}\left(1-\frac{1}{B}\right)\mathbf{P}\right] \tag{60}$$

Finally, the condition of zero stress normal to shell laminae is imposed considering $d\,\sigma^{33}=0$ in the rigitidy moduli of equation (60).

One should note that the consistent rigitity tensor in equation (60) is based on the assumption that tensors $\mathbf{s}^e$ and $\mathbf{s}_n$ are co-axial. If this assumption is not employed in the formulation, the following expression is obtained for the von Mises stress at the final state, instead of equation (51)

$$q_{n+1}=\frac{1}{1+\frac{3G}{h_{n+1}}}\left\{\left(\left(q^e\right)^2+\left(\frac{3G}{h_{n+1}}q_n\right)^2+\frac{6G}{h_{n+1}}Q^2\right)^{1/2}-\frac{3G\,H_{n+1}}{h_{1|n+1}}\Delta\varepsilon_q\right\} \tag{61}$$

and the correspoding consistent rigitity tensor has a more coplex form which is non-symmetric, as presented in Pappa (2014). In the present study, the consistent rigitity of equation (60) is employed.

3 LARGE STRAIN FORMULATION

In this section, the extension of the previous model for large strains is presented, towards efficient inelastic analysis of geometrically nonlinear shells based on an additive decomposition of the rate-of-deformation tensor.

Following a short presentation of the constitutive equations, their numerical intergation is described in detail.

3.1 Large-strain constitutive model

The starting point is a basic constitutive equation that relates the Jaumann rate of Kirchhoff stress $\boldsymbol{\tau}$ to the elastic part of rate-of-deformation tensor $\mathbf{d}$ by a linear hypoelastic equation of the form

$$\overset{\nabla}{\boldsymbol{\tau}} \equiv \dot{\boldsymbol{\tau}} + \boldsymbol{\tau}\,\mathbf{W} - \mathbf{W}\,\boldsymbol{\tau} = \mathbf{D}\mathbf{d}^{e} = \mathbf{D}\left(\mathbf{d} - \mathbf{d}^{p}\right) \tag{62}$$

where $\mathbf{W}$ is the spin tensor. Assuming von Mises plasticity with isotropic hardening, the yield criterion is defined by equation (8), where **s** is the deviatoric part of **τ,** and the flow rule is

$$\mathbf{d}^{p} = \frac{3}{2}\left(\frac{1}{E_s} - \frac{1}{E}\right)\overset{\nabla}{\mathbf{s}} + \frac{3}{2}\frac{\dot{q}}{q}\left(\frac{1}{E_T} - \frac{1}{E_s}\right)\mathbf{s} \tag{63}$$

which is an extension of the rate form of deformation theory for large strains (Neale 1981). In this equation, E_s and E_T are functions of the equivalent plastic strain ε_q, defined as the time integral of $\dot{\varepsilon}_q$

$$\dot{\varepsilon}_q = \sqrt{2/3}\;\mathbf{d}^{p}\cdot\mathbf{n} \tag{64}$$

an equation analogous to (9). Using a standard inversion procedure in equation (62), one obtains the elastic-plastic rigidity tensor $\mathbf{D}_{ep}$ so that

$$\overset{\nabla}{\boldsymbol{\tau}} = \mathbf{D}_{ep}\,\mathbf{d} \tag{65}$$

For the purposes of inserting the present model within a finite element formulation, to be discussed in the next section, the constitutive equation (65) is written in terms of the convected rate of Kirchhoff stress tensor $\overset{\circ}{\boldsymbol{\tau}}$ defined as follows

$$\overset{\circ}{\boldsymbol{\tau}} = \dot{\tau}^{ij}\left(\mathbf{g}_i \otimes \mathbf{g}_j\right) \tag{66}$$

From continuum mechanics (Malvern, 1969), one may show that the convected rate is related to the Jaumann rate as follows

$$\overset{\circ}{\boldsymbol{\tau}} = \overset{\nabla}{\boldsymbol{\tau}} - \mathcal{L}\,\mathbf{d} \tag{67}$$

where $\mathcal{L}$ is the geometric rigidity fourth-order tensor, with components:

$$\mathcal{L}^{ijkl} = \frac{1}{2}\left[\, g^{ik}\,\tau^{jl} + g^{jk}\,\tau^{il} + g^{il}\,\tau^{jk} + g^{jl}\,\tau^{ik}\,\right] \tag{68}$$

so that

$$\overset{\circ}{\boldsymbol{\tau}} = (\,\mathbf{D}_{ep} - \mathcal{L}\,)\mathbf{d} = \mathcal{R}\,\mathbf{d} \tag{69}$$

and $\mathcal{R}$ is a fourth order tensor, equal to:

$$\mathcal{R}^{ijkl} = D_{ep}^{ijkl} - \mathcal{L}^{ijkl} \tag{70}$$

It can be verified that the components of tensor $\mathcal{R}$ exhibit the symmetries $\mathcal{R}^{ijkl} = \mathcal{R}^{jikl} = \mathcal{R}^{ijlk}$ (due to symmetry of $\overset{\circ}{\boldsymbol{\tau}}$ and $\mathbf{d}$) and the nontrivial symmetry $\mathcal{R}^{ijkl} = \mathcal{R}^{klij}$.

3.2 Numerical integration of the large-strain model

To integrate the above constitutive equations, an equivalent expression of the equations in a "rotated" coordinate system is developed, using the rotation tensor $\mathbf{R}$ from the decomposition of the deformation gradient $\Delta\mathbf{F}$ that corresponds to the time step under consideration. This methodology has been first suggested by Nagtegaal (1982) and it is adjusted herein for the purpose of analyzing nonlinear shells. More specifically, the deformation gradient tensors at the beginning $\mathbf{F}_n$ and at the end $\mathbf{F}_{n+1}$ of the step are related as follows

$$\Delta\mathbf{F} = \mathbf{F}_{n+1}\mathbf{F}_n^{-1} = \mathbf{g}_i \otimes \mathbf{G}^i \tag{71}$$

where $\mathbf{g}_i$ are the covariant base vectors at the current configuration (end of the step), and $\mathbf{G}^i$ are the contravariant base vectors at the beginning of the step. Tensor $\Delta\mathbf{F}$ is decomposed into a stretch tensor $\mathbf{U}$ and a rotation tensor $\mathbf{R}$ so that

$$\Delta\mathbf{F} = \mathbf{R}\,\mathbf{U} \tag{72}$$

Tensors $\mathbf{R}$ and $\mathbf{U}$ refer to the step under consideration and should be regarded as incremental quantities from state n to state $n+1$. The stretch tensor $\mathbf{U}$ is the square root of the right Cauchy-Green tensor $\mathbf{C}$ (defined as $\mathbf{C} = \Delta\mathbf{F}^T\ \Delta\mathbf{F}$), and can be expressed in the following expression [Ting (1985); Hughes & Simo (1998)].

$$\mathbf{U} = A_1\mathbf{C}^2 + A_2\mathbf{C} + A_3\mathbf{1} \tag{73}$$

where $\mathbf{1}$ is the unit tensor, which can be written in the following form

$$\mathbf{1} = G_{ij}\left(\mathbf{G}^i \otimes \mathbf{G}^j\right) \tag{74}$$

tensor $\mathbf{C}^2$ is the square of the right Cauchy-Green tensor $\mathbf{C}$ defined as

$$\mathbf{C}^2 \equiv \mathbf{C}\mathbf{C} = g_{ik}g_{jl}G^{kj}\left(\mathbf{G}^i \otimes \mathbf{G}^l\right) \tag{75}$$

and A_i (i=1,2,3) depend on the principal invariants of $\mathbf{U}$, defined in Appendix II. An expression similar to equation (73) can be derived for the inverse tensor $\mathbf{U}^{-1}$ [Ting (1985); Hughes & Simo (1998)].

$$\mathbf{U}^{-1} = B_1\mathbf{C} + B_2\mathbf{U} + B_3\mathbf{1} \tag{76}$$

where B_i (i=1,2,3) depend on the principal invariants of $\mathbf{U}^{-1}$, also defined in Appendix II. From equations (73) and (76) the components of $\mathbf{U}$ and $\mathbf{U}^{-1}$ with respect to the $\left(\mathbf{G}^i \otimes \mathbf{G}^j\right)$ basis denoted as u_{ij}, $\overline{u}_{ij}$ respectively, are given by the following expressions

$$u_{ij} = A_1a_{ij} + A_2g_{ij} + A_3G_{ij} \tag{77}$$

$$\overline{u}_{ij} = B_1g_{ij} + B_2u_{ij} + B_3G_{ij} \tag{78}$$

where

$$a_{ij} = g_{ik}g_{jl}G^{kl} \tag{79}$$

Since $\mathbf{U}$ is symmetric and positive definite, the rotation tensor is written

$$\mathbf{R} = \Delta\mathbf{F}\ \mathbf{U}^{-1} \tag{80}$$

Therefore, the components of $\mathbf{R}$ with respect to the $\left(\mathbf{g}_k \otimes \mathbf{G}^j\right)$ basis are

$$r_j^k = \bar{u}_{ij} G^{ik} \tag{81}$$

so that

$$\mathbf{R} = r_j^k \left(\mathbf{g}_k \otimes \mathbf{G}^j\right) \tag{82}$$

Subsequently, the so-called rotated stress tensor $\hat{\boldsymbol{\tau}}$ and the logarithmic strain $\Delta\mathbf{E}$ are defined as follows

$$\hat{\boldsymbol{\tau}} = \mathbf{R}^T \boldsymbol{\tau}\, \mathbf{R} \tag{83}$$

$$\Delta\mathbf{E} = \ln \mathbf{U} \tag{84}$$

For computational purposes, a truncated Taylor series expression for the $\ln \mathbf{U}$ is considered

$$\ln \mathbf{U} = (\mathbf{U}-\mathbf{1}) - \frac{1}{2}(\mathbf{U}-\mathbf{1})^2 + \frac{1}{3}(\mathbf{U}-\mathbf{1})^3 + O(\mathbf{U}-\mathbf{1})^4 \tag{85}$$

where the higher-order terms are omitted. Combining equations (77), (84) and (85), the components of $\Delta\mathbf{E}$ with respect to $\mathbf{G}^i \otimes \mathbf{G}^i$ reference basis are

$$\Delta E_{ij} \cong u_{ij}^{(11)} - \frac{1}{2} u_{ik}^{(11)} u_{jm}^{(11)} G^{km} + \frac{1}{3} u_{ik}^{(12)} u_{jm}^{(11)} G^{km} \tag{86}$$

where

$$u_{ij}^{(11)} = u_{ij} - G_{ij} \tag{87}$$

$$u_{ij}^{(12)} = u_{ik}^{(11)} u_{jm}^{(11)} G^{km} \tag{88}$$

If the directions of the principal stretches (i.e., the eigenvectors of $\mathbf{U}$) remain fixed within the time period between t_n and t_{n+1}, it can be shown (Nagtegaal, 1982) that over that time period the following expressions can be written

$$\overset{\nabla}{\boldsymbol{\tau}} = \mathbf{R}\, \dot{\hat{\boldsymbol{\tau}}}\, \mathbf{R}^T \tag{89}$$

and

$$\dot{\mathbf{E}} = \mathbf{R}^T \mathbf{d}\, \mathbf{R} = \mathbf{R}^T \left(\mathbf{d}^e + \mathbf{d}^p\right) \mathbf{R} = \mathbf{R}^T \mathbf{d}^e\, \mathbf{R} + \mathbf{R}^T \mathbf{d}^p\, \mathbf{R} = \dot{\mathbf{E}}^e + \dot{\mathbf{E}}^p \tag{90}$$

where the elastic and plastic part of $\dot{\mathbf{E}}$ are defined as follows:

$$\dot{\mathbf{E}}^e = \mathbf{R}^T \mathbf{d}^e\, \mathbf{R} \tag{91}$$

$$\dot{\mathbf{E}}^p = \mathbf{R}^T \mathbf{d}^p\, \mathbf{R} \tag{92}$$

Using the above equations, the constitutive relation (62) and the flow rule (63) can be written for that time period in terms of the rotated stress and strain rates, as follows

$$\dot{\hat{\boldsymbol{\tau}}} = \mathbf{D}\dot{\mathbf{E}}^e = \mathbf{D}\left(\dot{\mathbf{E}} - \dot{\mathbf{E}}^p\right) \tag{93}$$

and

$$\dot{\mathbf{E}}^p = \frac{3}{2}\left(\frac{1}{E_s} - \frac{1}{E}\right)\dot{\hat{\mathbf{s}}} + \frac{3}{2}\frac{\dot{\hat{q}}}{\hat{q}}\left(\frac{1}{E_T} - \frac{1}{E_s}\right)\hat{\mathbf{s}} \tag{94}$$

where $\hat{q}$ is the von Mises equivalent stress of the rotated stress

$$\hat{q} = \sqrt{\frac{3}{2}\hat{\mathbf{s}}\cdot\hat{\mathbf{s}}} \tag{95}$$

One can readily show that

$$\hat{q} = \sqrt{\frac{3}{2}\mathbf{s}\cdot\mathbf{s}} = q \tag{96}$$

and

$$\dot{\hat{\varepsilon}}_q = \sqrt{\frac{2}{3}}\,\dot{\mathbf{E}}^p\cdot\hat{\mathbf{n}} \tag{97}$$

is equal to $\dot{\varepsilon}_q$, so that during plastic loading $\dot{\hat{q}} = \dot{\hat{\varepsilon}}_q H$. Using the rotated quantities of stress and strain, the hypoelastic equation (93) can be integrated exactly as follows

$$\hat{\boldsymbol{\tau}}_{n+1} = \boldsymbol{\tau}_n + \mathbf{D}\left(\Delta\mathbf{E} - \Delta\mathbf{E}^p\right) \tag{98}$$

where it was taken into account that $\hat{\boldsymbol{\tau}}_n = \boldsymbol{\tau}_n$. The above equations (93)-(98) are similar to the "small-strain" plasticity equations (1), (5)-(6), (9) and (20). Therefore, the integration of the elasto-plastic equations can be carried out by using a procedure similar to that described in the previous section for small-strain plasticity.

In addition, one should account for the condition of zero stress normal to the shell surface, requiring that throughout the analysis

$$\left(\boldsymbol{\tau}\,\mathbf{g}^3\right)\cdot\mathbf{g}^3 = \boldsymbol{\tau}\cdot\left(\mathbf{g}^3\otimes\mathbf{g}^3\right) = 0 \tag{99}$$

where $\mathbf{g}^3$ is the contravariant base vector normal to the shell laminae. Defining the "rotated basis" vectors $\hat{\mathbf{g}}^m$ and $\hat{\mathbf{g}}_j$ as

$$\hat{\mathbf{g}}_j = \mathbf{R}^T\mathbf{g}_j \tag{100}$$

$$\hat{\mathbf{g}}^m = \mathbf{R}^T\mathbf{g}^m \tag{101}$$

the zero normal stress condition (99) implies that

$$\left(\hat{\boldsymbol{\tau}}\,\hat{\mathbf{g}}^3\right)\cdot\hat{\mathbf{g}}^3 = \hat{\boldsymbol{\tau}}\cdot\left(\hat{\mathbf{g}}^3\otimes\hat{\mathbf{g}}^3\right) = 0 \tag{102}$$

or equivalently

$$\hat{\tau}^{33} = \hat{s}^{33} - \hat{p}\,\hat{g}^{33} = 0 \tag{103}$$

where $\hat{\tau}^{km}$ are the contravariant components of $\hat{\boldsymbol{\tau}}$ with respect to the $\hat{\mathbf{g}}_i$ basis, and from equations (81) and (101) one can readily show that

$$\hat{\mathbf{g}}^m = \bar{u}_{ij}G^{im}\mathbf{G}^j \tag{104}$$

Using an Euler-backward scheme for the integration of the flow rule (94), equation (93) becomes

$$\hat{\boldsymbol{\tau}}_{n+1} = \boldsymbol{\tau}_n + \mathbf{D}\Delta\mathbf{E} - 3G\left(\frac{1}{E_s}-\frac{1}{E}\right)\left(\hat{\mathbf{s}}_{n+1}-\hat{\mathbf{s}}_n\right) - 3G\,\frac{\dot{\hat{q}}}{\hat{q}}\left(\frac{1}{E_T}-\frac{1}{E_s}\right)\hat{\mathbf{s}}_{n+1} \tag{105}$$

Expressing tensors $\hat{\boldsymbol{\tau}}_n$, $\hat{\boldsymbol{\tau}}_{n+1}$, $\Delta\mathbf{E}$ in terms of tensor bases defined by the rotated vectors $\hat{\mathbf{g}}^m$, $\hat{\mathbf{g}}^k$

$$\Delta\mathbf{E} = \Delta\mathcal{E}_{km}\left(\hat{\mathbf{g}}^k \otimes \hat{\mathbf{g}}^m\right) \tag{106}$$

$$\hat{\boldsymbol{\tau}}_{n+1} = \hat{\tau}^{ij}_{n+1}\left(\hat{\mathbf{g}}_i \otimes \hat{\mathbf{g}}_j\right) \tag{107}$$

$$\hat{\boldsymbol{\tau}}_{n} = \hat{\tau}^{ij}_{n}\left(\hat{\mathbf{g}}_i \otimes \hat{\mathbf{g}}_j\right) \tag{108}$$

where

$$\Delta\mathcal{E}_{km} = \Delta E_{ij}\left(\mathbf{G}^i \cdot \hat{\mathbf{g}}_m\right)\left(\mathbf{G}^j \cdot \hat{\mathbf{g}}_k\right) \tag{109}$$

$$\hat{\tau}^{km}_{n+1} = \hat{\tau}^{ij}_{n+1}\left(\hat{\mathbf{g}}^k \cdot \mathbf{G}_j\right)\left(\hat{\mathbf{g}}^m \cdot \mathbf{G}_i\right) \tag{110}$$

so that equation (105) becomes

$$\hat{\tau}^{ij}_{n+1} = \hat{\tau}^{ij}_{n} + \hat{D}^{ijkm}\Delta\mathcal{E}_{km} - 3G\left(\frac{1}{E_s} - \frac{1}{E}\right)\left(\hat{s}^{ij}_{n+1} - \hat{s}^{ij}_{n}\right) - 3G\,\frac{\dot{\hat{q}}}{\hat{q}}\left(\frac{1}{E_T} - \frac{1}{E_s}\right)\hat{s}^{ij}_{n+1} \tag{111}$$

where $\hat{D}^{ijkm}$ are the components of the 4th order elastic rigidity tensor $\mathbf{D}$ with respect to the rotated basis $\hat{\mathbf{g}}_i \otimes \hat{\mathbf{g}}_j \otimes \hat{\mathbf{g}}_k \otimes \hat{\mathbf{g}}_l$. For the purposes of accounting for the zero stress condition normal to shell laminae, the strain increment is decomposed in a "known" and "unknown" part

$$\Delta\mathbf{E} = \Delta\,\overline{\mathbf{E}} + \Delta\,E_{33}\,\hat{\mathbf{a}} \tag{112}$$

where $\Delta\,\overline{\mathbf{E}}$ is the known part of the total strain increment $\Delta\mathbf{E}$ and

$$\hat{\mathbf{a}} = \hat{\mathbf{g}}^{\mathbf{3}} \otimes \hat{\mathbf{g}}^{\mathbf{3}} = \hat{g}^{3k}\hat{g}^{3m}\left(\hat{\mathbf{g}}_k \otimes \hat{\mathbf{g}}_m\right) \tag{113}$$

so that

$$\hat{\boldsymbol{\tau}}_{n+1} = \hat{\bar{\boldsymbol{\tau}}}^{e} + \Delta E_{33}\left(\mathbf{D}\hat{\mathbf{a}}\right) - 3G\left(\frac{1}{E_s} - \frac{1}{E}\right)\left(\hat{\mathbf{s}}_{n+1} - \hat{\mathbf{s}}_{n}\right) - 3G\,\frac{\dot{\hat{q}}}{\hat{q}}\left(\frac{1}{E_T} - \frac{1}{E_s}\right)\hat{\mathbf{s}}_{n+1} \tag{114}$$

where

$$\hat{\bar{\boldsymbol{\tau}}}^{\,e} = \boldsymbol{\tau}_n + \mathbf{D}\Delta\,\overline{\mathbf{E}} \tag{115}$$

The solution algorithm proceeds exactly as described in section 2.2 for small strains considering the “rotated” base vectors $\hat{\mathbf{g}}_i$, $\hat{\mathbf{g}}_j$ and that $\hat{\boldsymbol{\tau}}^{33}_{n+1} = 0$. Upon calculations of $\hat{\tau}^{ij}_{n+1}$, i.e., the components of tensor $\hat{\boldsymbol{\tau}}$ with respect to the «rotated» base $\left(\hat{\mathbf{g}}_i \otimes \hat{\mathbf{g}}_j\right)$, the components τ^{pm}_{n+1} of tensor $\hat{\boldsymbol{\tau}}_{n+1}$ with respect to the current base $\left(\mathbf{g}_p \otimes \mathbf{g}_m\right)$ should be computed, using the definition of $\hat{\boldsymbol{\tau}}$. More specifically, the final stress is

$$\boldsymbol{\tau}_{n+1} = \mathbf{R}\hat{\boldsymbol{\tau}}_{n+1}\mathbf{R}^T \tag{116}$$

After some tensor algebra using equation (81)

$$\boldsymbol{\tau}_{n+1} = r^q_p r^m_k \hat{\tau}^{ij}_{n+1}\left(\hat{\mathbf{g}}_i \cdot \mathbf{G}^q\right)\left(\hat{\mathbf{g}}_j \cdot \mathbf{G}^p\right)\left(\mathbf{g}_p \otimes \mathbf{g}_m\right) \tag{117}$$

and therefore the components of the final stress with respect to the current covariant basis can be computed as follows:

$$\tau^{pm}_{n+1} = r^q_p r^m_k \left(\hat{\mathbf{g}}_i \cdot \mathbf{G}^q\right)\left(\hat{\mathbf{g}}_j \cdot \mathbf{G}^p\right)\hat{\tau}^{ij}_{n+1} \tag{118}$$

4 FINITE ELEMENT FORMULATION

The above constitutive model is suitable for the nonlinear analysis of any type of shell, with double curvature. In the present work, it is implemented within a special-purpose nonlinear finite element technique for the analysis and buckling of cylindrical and tubular shells. The nonlinear formulation adopted in the present work was introduced in its general form by Needleman (1982). It has been employed for the nonlinear analysis of relatively thick elastic-plastic offshore tubular members (Karamanos and Tassoulas 1996) and, more recently, for the elastic stability of thin-walled cylinders under bending and pressure (Karamanos, 2002; Houliara and Karamanos, 2006, 2010).

The cylindrical shell is considered as an elastic-plastic continuum with embedded (convected) coordinates are denoted by ξ^i $(i=1,2,3)$, as described in previous sections. The position vector of the material point (ξ^1,ξ^2,ξ^3) in the current (deformed) configuration at time t is denoted as $\mathbf{x}=\mathbf{x}(\xi^1,\xi^2,\xi^3,t)$, whereas the position of the material point (ξ^1,ξ^2,ξ^3) at t =0 in the reference (undeformed) configuration is denoted by $\mathbf{X}=\mathbf{X}(\xi^1,\xi^2,\xi^3)$. At any material point, the covariant base vectors in the reference and in the current configuration, which are tangent to the coordinate lines, are $\tilde{\mathbf{G}}_i=\partial\mathbf{X}/\partial\xi^i$ and $\mathbf{g}_i=\partial\mathbf{x}/\partial\xi^i$, respectively. Furthermore, $\tilde{\mathbf{G}}^k$ and $\mathbf{g}^k$ denote the contravariant (reciprocal) base vectors in the reference and current configuration, respectively.

4.1 Governing equations

The constitutive equations, extensively discussed in the previous section, relate the convected rate of Kirchhoff stress tensor $\overset{\circ}{\boldsymbol{\tau}}$ to the rate of deformation tensor $\mathbf{d}$ through the relationship

$$\overset{\circ}{\boldsymbol{\tau}}=\left(\mathbf{D}_{ep}-\mathcal{L}\right)\mathbf{d}=\mathcal{R}\,\mathbf{d} \tag{119}$$

where $\mathbf{D}_{ep}$ is the elastoplastic rigidy fourth-order tensor and $\mathcal{L}$ is the geometric rigidity fourth-order tensor. Expressions for the components of $\mathbf{D}_{ep}$, $\mathcal{L}$ and $\mathcal{R}$ are offered in equations (16), (68) and (70) respectively.

Deformation is described by the rate-of-deformation (stretch) tensor $\mathbf{d}$, which is the symmetric part of the velocity gradient. It can be shown that the covariant components of the rate-of-deformation tensor are:

$$d_{kl}=\frac{1}{2}\left(V_{m/l}(\tilde{\mathbf{G}}^m\cdot\mathbf{g}_k)+V_{m/k}(\tilde{\mathbf{G}}^m\cdot\mathbf{g}_l)\right) \tag{120}$$

where $V_{m/l}$ is the covariant derivative of the velocity vector component V_m with respect to the reference basis.

Equilibrium is expressed through the principle of virtual work, considering an admissible displacement field $\delta\mathbf{u}$. For a continuum occupying the region V_0 and V in the reference and in the current configuration, respectively, and with boundary B in the deformed configuration, the principle of virtual work is expressed as:

$$\int_{V_0}\delta U_{i/j}(\tilde{\mathbf{G}}^{\mathrm{i}}\cdot\mathbf{g}_{\mathrm{k}})\,\tau^{kj}dV_0=\int_B\delta\mathbf{u}\cdot\mathbf{t}\,dB_q \tag{121}$$

where $\mathbf{t}$ is the surface traction and τ^{ij} are the contravariant components of the Kirchhoff stress tensor $\boldsymbol{\tau}$, which is parallel to the Cauchy stress $\boldsymbol{\sigma}$ ($\boldsymbol{\tau}\,dV_0=\boldsymbol{\sigma}\,dV$) and

$$\delta U_{i/j}=\frac{\partial(\delta\mathbf{u})}{\partial\xi^j}\cdot\tilde{\mathbf{G}}_{\mathrm{i}} \tag{122}$$

For the purpose of linearizing the equilibrium equations, the principle of virtual work is considered at a "nearby"

configuration $\mathbf{x}'\left(\xi^1,\xi^2,\xi^3\right)$

$$\int_{V_0}\delta U'_{k/j}\left(\tilde{\mathbf{G}}^k\cdot\mathbf{g}'_i\right)\tau'^{ij}dV_0=\int_{B'}\delta\mathbf{u}'\cdot\mathbf{t}'\,dB' \tag{123}$$

corresponding to boundary B', stress tensor $\boldsymbol{\tau}'$ and boundary traction $\mathbf{t}'$. Considering the increment of displacement $\Delta\mathbf{u}$, defined as the difference between, vectors $\mathbf{x}'$ and $\mathbf{x}$ and the linearized form of the principle of virtual work is obtained as follows

$$\int_{V_0}\delta U_{i/j}\,S^{ijpq}\,\Delta U_{p/q}\,dV_0=\int_{B}\delta\mathrm{u}\cdot\mathrm{t}'\,dB-\int_{V_0}\delta U_{i/j}\,\hat{\sigma}^{ji}\,dV_0 \tag{124}$$

where

$$\Delta U_{p/q}=\frac{\partial\left(\Delta\mathrm{u}\right)}{\partial\xi^q}\cdot\tilde{\mathbf{G}}_p \tag{125}$$

components S^{ijpq} refer to the fourth-order tensor $\mathbf{S}$ and are equal to

$$S^{ijpq}=\left(\tilde{\mathbf{G}}^i\cdot\mathbf{g}_k\right)R^{kjmq}\left(\mathbf{g}_m\cdot\tilde{\mathbf{G}}^p\right)+\tau^{jq}\,\tilde{G}^{ip} \tag{126}$$

and $\hat{\sigma}^{ij}$ are the contravariant components of the non-symmetric nominal stress tensor $\hat{\boldsymbol{\sigma}}$, defined as follows:

$$\hat{\boldsymbol{\sigma}}=\frac{dV}{dV_0}\mathbf{F}^{-1}\boldsymbol{\sigma} \tag{127}$$

or, in component form

$$\hat{\sigma}^{ij}=\tau^{ij}\left(\mathbf{g}_k\cdot\tilde{\mathbf{G}}^j\right) \tag{128}$$

4.2 Finite element discretization and implementation

Using a finite element discretization and adopting matrix notation, the incremental displacement field can be expressed as

$$\Delta\mathbf{u}=[\mathbf{N}]\Delta\hat{\mathbf{U}} \tag{129}$$

in which [**N**] is the interpolation matrix that contains the appropriate shape functions and $\Delta\hat{\mathbf{U}}$ is a vector that contains the increments of nodal degrees of freedom. Using the same functions for the virtual displacements, one can write

$$\delta\mathbf{u}=[\mathbf{N}]\delta\hat{\mathbf{U}} \tag{130}$$

where $\delta\hat{\mathbf{U}}$ are arbitrary virtual nodal displacements.

The covariant differentiation of equations (129) and (130) results in:

$$grad(\Delta\mathbf{u})=\left\{\Delta U_{k/l}\right\}=[\mathbf{B}]\Delta\hat{\mathbf{U}} \tag{131}$$

$$grad(\delta\mathbf{u})=\left\{\delta U_{k/l}\right\}=[\mathbf{B}]\delta\hat{\mathbf{U}} \tag{132}$$

where [**B**] contains the derivatives of the elements of the interpolation matrix. Furthermore, in matrix form, equation (126) becomes,

$$\left[\mathbf{S}\right]=\left[\mathbf{W}\right]^T\left[\mathfrak{R}\right]\left[\mathbf{W}\right]+\left[\mathbf{C}\right] \tag{133}$$

where $[\mathbf{W}]$ is a matrix containing the mixed components of the deformation gradient with respect to the reference base vectors

$$\mathrm{F}^{i}_{\cdot j} = \mathbf{F}\cdot\left(\tilde{\mathbf{G}}^{i}\otimes\tilde{\mathbf{G}}_{j}\right) = \left(\mathbf{F}\tilde{\mathbf{G}}_{j}\right)\cdot\tilde{\mathbf{G}}^{i} = \tilde{\mathbf{G}}^{i}\cdot\mathbf{g}_{j} \tag{134}$$

and $[\mathfrak{R}]$ contains the components of rigidity tensor $\mathfrak{R}$ defined in (70).

For arbitrary virtual displacements $\delta\hat{\mathbf{U}}$ the following set of linearized equations of the discretized continuum is obtained:

$$[\mathbf{K}]\Delta\hat{\mathbf{U}} = \mathbf{F}_{ext} - \mathbf{F}_{int} \tag{135}$$

where $[\mathbf{K}]$ is the incremental stiffness matrix

$$[\mathbf{K}] = \int_{V_0}[\mathbf{B}]^{T}[\mathbf{S}][\mathbf{B}]dV_0 \tag{136}$$

and $\mathbf{F}_{ext}$, $\mathbf{F}_{int}$ are the external and internal load vectors respectively:

$$\mathbf{F}_{ext} = \int_{B_q}[\mathbf{N}]^{T}\mathbf{t}'dB_q \tag{137}$$

$$\mathbf{F}_{int} = \int_{V_0}[\mathbf{B}]^{T}[\mathbf{W}]^{T}\boldsymbol{\tau}dV_0 \tag{138}$$

Equilibrium is achieved when $\mathbf{F}_{int}$ equals $\mathbf{F}_{ext}$. An incremental Newton-Raphson iterative numerical procedure is employed, enhanced to enable the tracing of postbuckling "snap-back" equilibrium paths through an arc-length algorithm, which monitors the value of the so-called "arc-length parameter" (Crisfield, 1983).

The cylinder is discretized through a three-node "tube element" (see Figure 3), introduced in Karamanos and Tassoulas (1996) for the analysis of thick walled tubes also employed for analysis of thin-walled elastic cylinders. This element combines longitudinal (beam-type) with cross-sectional deformation. The convected coordinates $\left(\xi^1,\xi^2,\xi^3\right)$ are assumed in the hoop, axial and radial direction in the reference configuration respectively and are denoted as (θ,ζ,ρ).

Nodes are located along the cylinder axis, which lies on the plane of bending, and each node possesses three degrees of freedom (two translational and one rotational). A reference line is chosen within the cross-section at node (k) and a local Cartesian coordinate system is defined, so that the $\bar{x},\bar{y}$ axes define the cross-sectional plane. The orientation of node (k) is defined by the position of three orthonormal vectors $\mathbf{e}_x^{(k)}$, $\mathbf{e}_y^{(k)}$ and $\mathbf{e}_z^{(k)}$. For in-plane (ovalization) deformation, fibers initially normal to the reference line remain normal to the reference line. Furthermore, those fibers may rotate in the out-of-plane direction by angle $\gamma(\theta)$. Using quadratic interpolation in the longitudinal direction, the position vector $\mathbf{x}(\theta,\zeta,\rho)$ of an arbitrary point at the deformed configuration is:

$$\mathbf{x}(\theta,\zeta,\rho) = \sum_{k=1}^{3}\left[\left(\mathbf{x}^{(k)} + \mathbf{r}^{(k)}(\theta) + \rho\mathbf{n}^{(k)}(\theta) + \rho\gamma(\theta)\mathbf{e}_z^{(k)}\right)N^{(k)}(\zeta)\right] \tag{139}$$

where $\mathbf{x}^{(k)}$ is the position vector of node (k), $\mathbf{r}^{(k)}(\theta)$ is the position of the reference line at a certain cross-section relative to the corresponding node (k), $\mathbf{n}^{(k)}(\theta)$ is the "in-plane" outward normal of the reference line at

the deformed configuration and $N^{(k)}(\zeta)$ is the corresponding Lagrangian quadratic polynomial. Using nonlinear ring theory (Brush and Almroth, 1975), vector functions $\mathbf{r}^{(k)}(\theta)$ and $\mathbf{n}^{(k)}(\theta)$, can be expressed in terms of the radial, tangential and out-of-plane displacements of the reference line, denoted as $w(\theta)$, $v(\theta)$, $u(\theta)$, respectively. Functions $w(\theta)$, $v(\theta)$, $u(\theta)$ and $\gamma(\theta)$ are discretized as follows:

$$w(\theta) = a_0 + a_1 \sin\theta + \sum_{n=2,4,6,...} a_n \cos n\theta + \sum_{n=3,5,7,....} a_n \sin n\theta \tag{140}$$

$$v(\theta) = -a_1 \sin\theta + \sum_{n=2,4,6,...} b_n \sin n\theta + \sum_{n=3,5,7,....} b_n \cos n\theta \tag{141}$$

$$u(\theta) = \sum_{n=2,4,6,...} c_n \cos n\theta + \sum_{n=3,5,7,....} c_n \sin n\theta \tag{142}$$

$$\gamma(\theta) = \sum_{n=0,2,4,6,...} \gamma_n \cos n\theta + \sum_{n=1,3,5,7,....} \gamma_n \sin n\theta \tag{143}$$

Coefficients a_n, b_n refer to in-plane cross-sectional deformation, and express the ovalization of the cross-section, whereas c_n, γ_n refer to out-of-plane cross-sectional deformation, expressing cross-sectional warping.

For the purposes of the present study, a 16th degree expansion is used for $w(\theta)$, $v(\theta)$, $u(\theta)$ and $\gamma(\theta)$ [considering $n \leq 16$ in equations (140)-(143)], and four "tube-elements" per half wavelength are employed. Regarding the number of integration points, 23 equally spaced integration points around the half-circumference, five Gauss points in the radial (through the thickness) direction and two Gauss points in the longitudinal direction of the "tube element" are considered (reduced integration scheme) following relevant convergence studies reported in previous works of senior author (Karamanos, 2002; Houliara & Karamanos, 2010).

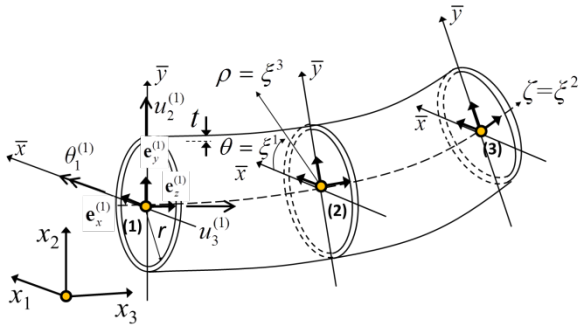

Figure 3: Three-node "tube element".

4.3 Bifurcation in the inelastic range

Detection of bifurcation from prebuckling to post-buckling is performed upon convergence of solution at the end of each loading increment, adopting Hill's "comparison solid" concept, as described in detail by Hutchinson (1974). The use of "comparison solid" yields lower bound, yet quite accurate, estimates of the bifurcation load, introducing the quadratic functional F:

$$F = \int_V (R^{ijkl} \Delta E_{ij} \Delta E_{kl} + \tau^{ij} \Delta U^k_{/j} \Delta U_{k/j}) dV \tag{144}$$

The positive definiteness of functional (144) ensures uniqueness of solution and stability. At the stage where F becomes non-positive definite, bifurcation occurs. Using the following expressions,

$$\tau^{ij}\Delta U^{k}_{/j}\Delta U_{k/j} = \tau^{ij}\Delta U_{m/j}\,\tilde{G}^{mk}\,\Delta U_{k/j} \tag{145}$$

$$\Delta E_{ij} = \frac{1}{2}\left[\left(\tilde{\mathbf{G}}^{k}\cdot\mathbf{g}_{p}\right)\Delta U_{k/q} + \left(\tilde{\mathbf{G}}^{k}\cdot\mathbf{g}_{q}\right)\Delta U_{k/p}\right] \tag{146}$$

and the finite element discretization procedure described in the previous paragraphs, functional F can be written in the following quadratic form in terms of "stiffness matrix" $[\mathbf{K}']$

$$F = \Delta\hat{\mathbf{U}}^{T}[\mathbf{K}']\Delta\hat{\mathbf{U}} \tag{147}$$

where

$$[\mathbf{K}'] = \int_{V_0}[\mathbf{B}]^{\mathrm{T}}[\mathbf{S}][\mathbf{B}]dV_0 \tag{148}$$

and

$$[\mathbf{S}] = [\mathbf{W}]^{\mathrm{T}}[\mathcal{R}'][\mathbf{W}] + [\mathbf{C}] \tag{149}$$

and $[\mathcal{R}']$ is the constitutive matrix containing the tangent elastic-plastic moduli $\mathcal{R}^{ijkl}$ of J_2-non associative flow theory moduli. Therefore, the positive definiteness of F is equivalent to the positive definiteness of $[\mathbf{K}']$, examined through the evaluation of its eigenvalues at the end of each loading increment. Bifurcation occurs when the smallest eigenvalue of $[\mathbf{K}']$ becomes equal to zero.

5 CONTINUITY OF PLASTIC FLOW

To quantify the production of plastic flow, the so-called plastic production ratio is adopted (Hughes and Shakib, 1986), defined as:

$$w(\theta) = \left\|\dot{\mathbf{e}}^{p}\right\| \Big/ \left\|\dot{\mathbf{e}}\right\| \tag{150}$$

where $\dot{\mathbf{e}}$ is the deviatoric part of incremental strain tensor $\dot{\boldsymbol{\varepsilon}}$, and $\dot{\mathbf{e}}^{p}$ is the plastic part of $\dot{\mathbf{e}}$. Equivalently, equation (150) can be written in a normalized form:

$$w^{*} = w\left(1+\frac{H}{3G}\right) \tag{151}$$

offering a measure of plastic strain-rate dependence on the direction of strain increment with respect to the outward unit normal to the yield surface $\mathbf{n}$. The value of w depends on angle θ between the outward normal $\mathbf{n}$ and the deviatoric strain increment $\dot{\mathbf{e}}$:

$$\cos\theta = \frac{\left(\mathbf{n}\cdot\dot{\mathbf{e}}\right)}{\left\|\dot{\mathbf{e}}\right\|} \tag{152}$$

In classical plasticity, loading paths tangential to the yield surface $(\theta = \pi/2)$ imply zero platic deformation, so that $w^{*} = 0$ for $\theta \geq \pi/2$, as a result of elastic behavior. This shown in Figure 4 for J_2-flow theory, as well as for the models proposed by Hughes and Shakib (1986) and Simo (1987).

For the non-associative flow rule under consideration as expressed in equation (10) and using the definition of plastic production ratio in equation (150), the following expression for the plastic production ratio is obtained:

$$w^*(\theta)=\left(1+\frac{H}{3G}\right)\sqrt{A+B\cos^2\theta} \tag{153}$$

where

$$A=1\Big/\left(1+h\left(\varepsilon_q\right)\Big/3G\right)^2 \tag{154}$$

$$B=1\Big/\left(1+H/3G\right)^2-1\Big/\left(1+h\left(\varepsilon_q\right)\Big/3G\right)^2 \tag{155}$$

In Figure 4 the value of w^* from present model, expressed in equations (153) - (155) is also plotted in terms of angle θ with the continuous lines. The two lines corresponds to two levels of equivalent plastic strain ε_q equal to 2% and 5% respectively. There exists a discontinuity at $\theta=\pi/2$, which is due to the non-zero tangential component of $\dot{\boldsymbol{\varepsilon}}^p$. Apart from the fact that this discontinuity is not consistent with the physical problem, it may cause numerical convergence problems. Therefore, a zero value of $w^*=0$ at $\theta=\pi/2$ is desired, and a modification of the plastic flow equation (5) is proposed, so that the tangential (non-associative) part of the right-hand side vanishes for θ values approaching $\pi/2$. Towards this purpose, a modified value of the secant modulus E_s is considered in terms of θ, denoted as $\bar{E}_s$, as follows:

$$\bar{E}_s\left(\varepsilon_q\right)=E_s\left(\varepsilon_q\right)\left(1-sin^{\mathrm{n}}\,\theta\right)+E\left(sin^{\mathrm{n}}\,\theta\right),\ \theta\ge\theta_0 \tag{156}$$

where θ_0 is a threshold value quite close to $\pi/2$ and n is a large-valued exponent. Therefore,

$$\bar{h}\left(\varepsilon_q\right)=\frac{E\bar{E}_s\left(\varepsilon_q\right)}{E-\bar{E}_s\left(\varepsilon_q\right)} \tag{157}$$

and the plastic ratio becomes a continuous function of θ, approaching smoothly the value of $\pi/2$.This is shown in Figure 4 with the dotted lines for values of θ_0 and n equal to 75º and 300 respectively. In such a case,

$$\bar{w}^*(\theta)=\left(1+\frac{H}{3G}\right)\sqrt{\bar{A}+\bar{B}\cos^2\theta} \tag{158}$$

$$\bar{A}=1\Big/\left(1+\bar{h}\left(\varepsilon_q\right)\Big/3G\right)^2 \tag{159}$$

$$\bar{B}=1\Big/\left(1+H/3G\right)^2-1\Big/\left(1+\bar{h}\left(\varepsilon_q\right)\Big/3G\right)^2 \tag{160}$$

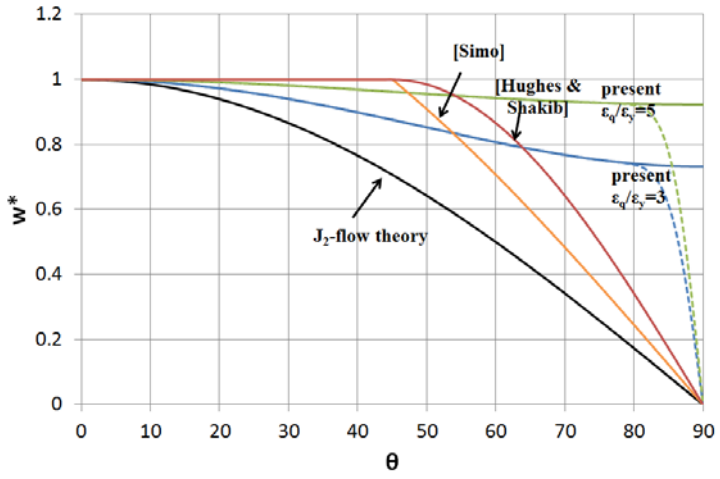

Figure 4: Variation of normalized plastic production ratio w^* in terms of θ for various plasticity models.

6 VERIFICATION RESULTS

Numerical results for benchmark problems of metal cylindrical shell buckling are obtained to validate the numerical methodology described in the previous sections. Large-strains are considered with the material model formulation described in section 3. Furthermore, the integration of constitutive models is performed with the Euler-backward method described in section 2.2.

6.1 Wrinkling of axially-compressed cylinders

The first problem refers to wrinkling of stainless steel tubes under uniform axial compression, and comparison with both experimental data and analytical predictions is conducted. Bifurcation analysis of perfect cylinders, associated with the initial development of wrinkles is described first. Subsequently, simulation of gradual development and localization of wrinkles in initially imperfect cylinders is presented using a nonlinear incremental analysis.

The tubes under consideration have been tested by Bardi and Kyriakides (2006) and are made of stainless steel material SAF 2507 super-duplex, which can be described for uniaxial tension through a Ramberg-Osgood stress-strain curve [eq. (161)]

$$\varepsilon = \frac{\sigma}{E}\left[1+\frac{3}{7}\left(\frac{\sigma}{\bar{\sigma}}\right)^{n+1}\right] \tag{161}$$

The values of E, $\bar{\sigma}$ and n have been determined through an appropriate tensile test equal to 194 GPa, 572 MPa and 13 respectively. The cylindrical shells are thick-walled with diameter-to-thickness ratio between 20 and 50, and are appropriately machined so that the buckling area can be considered free of boundary conditions. More details on the specimens and the experimental procedure can be found in Bardi & Kyriakides (2006).

Initial wrinkling of those tubes as obtained from a bifurcation analysis conducted with the present numerical tools. The numerical results are compared with experimental results and analytical solutions. More specifically, the bifurcation load at first wrinkling can be calculated analytically using the following equation (Batterman, 1965; Bardi & Kyriakides, 2006).

$$\sigma_{cr} = \left[\frac{C_{11}C_{22} - C_{12}^2}{3}\right]^{1/2} \left(\frac{t_s}{R}\right) \tag{162}$$

where R and t_s are the radius and wall thickness of the tube and $C_{a\beta}$ are the instantaneous material moduli for plane stress conditions, at the bifurcation stage. Expressions for moduli $C_{a\beta}$, for both associative and non-assocative J_2-plasticity, can be found in Bardi and Kyriakides (2006). It should be noted that first wrinkling of those thick-walled cylinders in the plastic range is always axisymmetric (Figure 6) as shown analytically by Gellin (1979).

The analytical and numerical predictions for the critical stress and strain are plotted against D/t_s in Figure 5, together with experimental results reported in Bardi et al. (2006). In this figure, ○ and ● refer to the upper and lower bound of first wrinkling observed in tests (Bardi and Kyriakides, 2006) respectively. In the same graph, the corresponding predictions using J_2-flow (associative) and the present (non-associative) theory both analytically and numerically are also shown. Note that the numerical predictions of J_2-flow theory have been obtained from the present finite element technique and the constitutive equations for the associative flow rule; these equations are obtained from the flow rule (10) omitting the second term on the right-hand-side and are reported in Pappa (2014). The analytical predictions are obtained from equation (162) using the appropriate instantaneous moduli $C_{a\beta}$ for the associative and non-associative case. The comparison with experimental data shows the superiority of the non-associative flow model with respect to the associative flow model in predicting bifurcation in the plastic range. Furthermore, a very good comparison of the present numerical model and the corresponding analytical results from equation (162) is shown. The axisymmetric buckling shape is depicted in Figure 6.

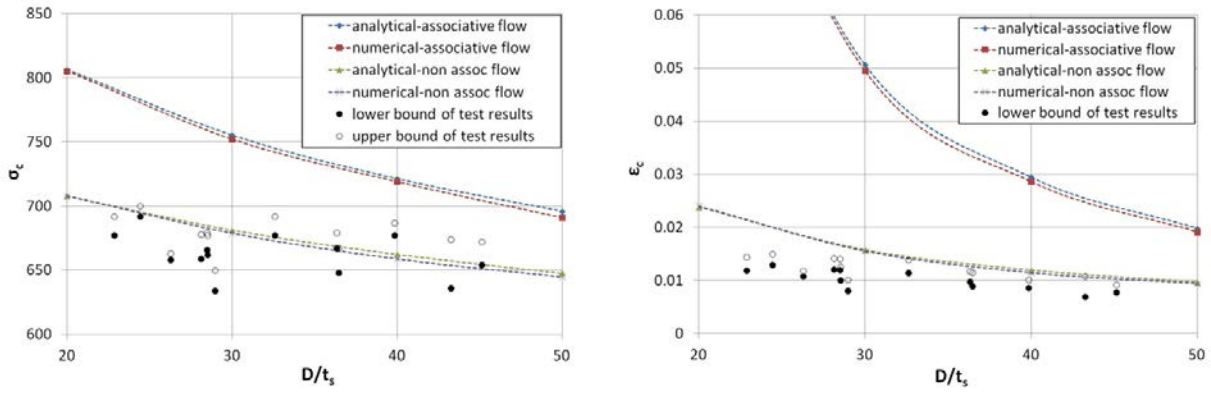

(a) (b)

Figure 5: (a) Critical stress (onset of wrinkling) vs. specimen D/t_s and (b) critical strain vs. specimen D/t_s, analytical predictions refers to equation (162).

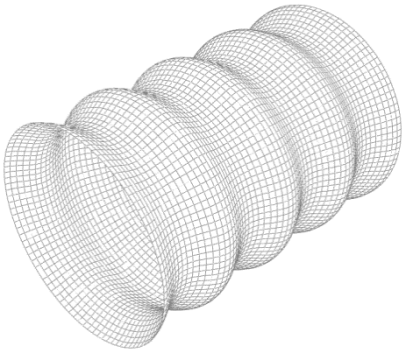

Figure 6: Bifurcation (first wrinkling) shape of axially loaded stainless steel cylinder (D/t_s =26.3).

Following the above bifurcation analysis, a nonlinear analysis is performed that follows the gradual development of wrinkles under increasing axial compression. Thick-walled cylinders subjected to axial compression, exhibit limit load instability (occurrence of maximum load on the load-displacement curve), followed by the development of localized buckling patterns. To describe this process, an initially axisymmetrically wrinkled pattern is assumed and gradual development and localization of this wrinkling pattern is monitored. Towards this purpose, a thick-walled cylinder (D/t_s =26.3), with the same material is considered, using a tube segment of length equal to seven half-wavelengths. Each half-wavelength corresponds to the first buckling shape of Figure 6, and an initial wave-type imperfection is imposed with a small amplitude $\omega_{0,max}$ equal to 0.1% of thickness. The half-wave length L_{hw} has been determined from the bifurcation analysis described above, equal to 14.515 mm. The load-displacement equilibrium path is shown in Figure 7a. Considering a small bias in the amplitude of one wrinkle (as initial imperfection), the analysis leads to a maximum load due to wrinkle localization denoted as limit state as shown in Figure 7a, where the numerical analysis the experimental curve are compared. The comparison between the non-associative model and tests results is very good in terms of the maximum load, the corresponding deformation and the initial post buckling behavior. It is noted that the limit (maximum) load occurs at a value of imposed displacement δ/L equal to 4.5%, which is well beyond the strain at which first wrinkles occur in the perfect cylinder (1.8%), shown in Figure 5b. This means that first bifurcation may not be related to the ultimate axial compression capacity of the cylinder, as noted by Bardi and Kyriakides (2006). Figure 7b shows the buckled configuration of the cylindrical shell and the localization of wrinkling deformation at a value of imposed displacement δ/L equal 5%. In Figure 7c the evolution of radial displacement along a cylinder generator is shown, illustrating the non-uniform growth of wrinkle amplitude; the central ripple grows significantly more than the others, resulting in localization of wrinkled pattern and loss of structural strength. Finally, in Figure 7a, the numerical results using the classical J_2-flow theory are also shown. The comparison is satisfactory up to a certain level, but this associative model does not predict accurately the ultimate load deformation and the initial post buckling behavior.

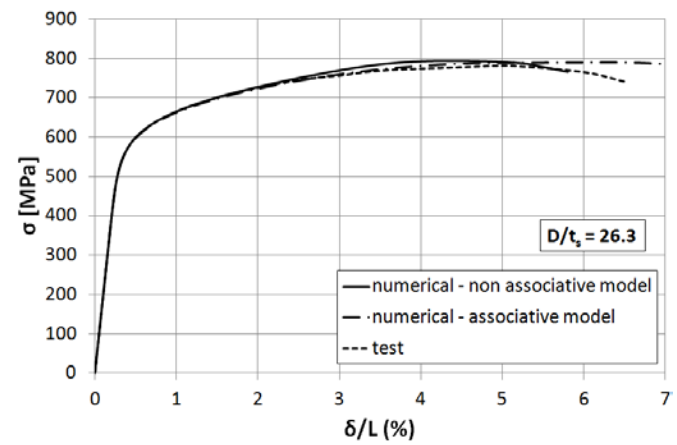

(a)

(b)

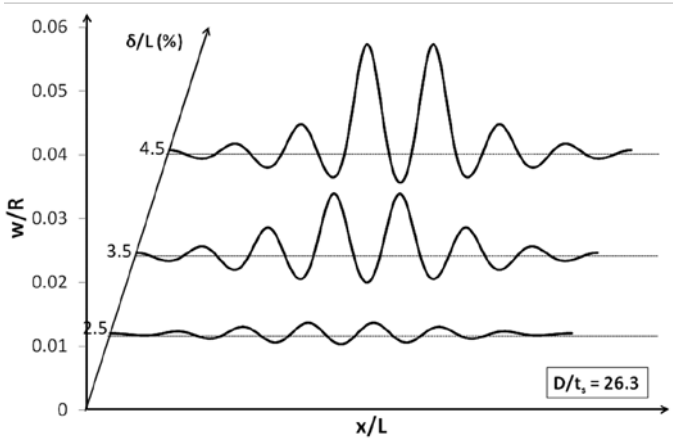

(c)

Figure 7: (a) Stress-displacement response, comparison with the test result reported in Bardi & Kyriakides (2006); (b) Deformed configuration of axially loaded cylinder with localized wrinkling corresponding to δ/L value of 5%; (c) evolution of radial displacement along a cylinder generator with increasing axial compression.

6.2 Buckling of imperfect axially-compressed cylinders

The buckling performance of imperfect thick-walled cylinders subjected to axial (meridional) compression has been examined analytically by Gellin (1979). Gellin enhanced the methodology initially proposed by Koiter (1963) for elastic thin-walled cylinders, employing shell kinematics based on DMV shell theory, and elastic-plastic material behavior through J_2 deformation theory.

Comparison is conducted for a moderately thin-walled cylindrical shell with D/t_s equal to 51. The material behavior can be described by equation (161), with E, $\bar{\sigma}$ and n equal to 194 GPa, 572 MPa and 5 respectively, so that the ratio of the effective yield stress $\bar{\sigma}$ to the classical buckling stress of the elastic shell $\bar{\sigma}/\sigma_c^e$ is 0.5 (σ_c^e is defined equal to $E t_s \Big/ \sqrt{3\left(1-\nu^2\right)}\, R$). The analysis assumes an initial imperfection in the form of first axisymmetric buckling mode (see Figure 6) obtained by a bifurcation analysis, as described above.

Considering a tube segment of length equal to twice the value of half-wavelength ($L = 2L_{hw}$), and the

axisymmetric initial imperfection, secondary bifurcation to a non-axisymmetric mode is calculated. The results of the numerical calculations are presented in Figure 8, where the bifurcation load of the imperfect shell P_{cr} is normalized by the bifurcation load of the perfect shell $P_{cr,0}$ and plotted in terms of the imperfection amplitude $\omega_{0,max}$ showing a very good comparison with Gellin's results.

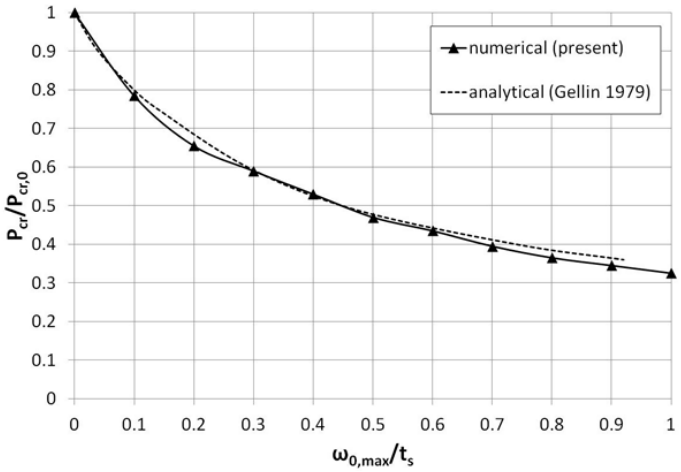

Figure 8: Imperfection sensitivity in the plastic range for a metal cylinder with D/t_s =51 and yield stress 572 MPa.

6.3 Bending of elongated metal cylinders

The third problem refers to an elongated cylindrical shell, referred to as "tube", subjected to longitudinal bending. The tube is made of aluminum (AL 6061-T6), diameter and thickness are equal to 31.75 mm (1.25 in) and 0.889 mm (0.035 in) respectively, (D/t_s =35.7) and has been tested experimentally (Kyriakides and Ju, 1992). Material behavior is described by a Ramberg-Osgood of stress-strain curve equation (161), with E, $\bar{\sigma}$ and n equal to 67.36 GPa, 282 MPa and 28 respectively, corresponding to a yield stress of 283.4 MPa .

The structural response of thick cylindrical shells and the ensuing instabilities are strongly influenced by the plastic behavior of the metal material, as well as by the ovalization of the cross-section, implying a highly nonlinear prebuckling state. Along this nonlinear path, the shell exhibits various shell-type buckling modes in the form of wrinkles along its compression side. First bifurcation occurs in a uniform wrinkling pattern shown in Figure 9 denoted by the first arrow (↑) on the primary path, which is similar to the first wrinkling pattern reported in the tests of Kyriakides and Ju (1992) and a second bifurcation on the same prebuckling path is also detected, in the form shown in Figure 9 denoted by the second arrow (↑). The moment is normalized by the fully-plastic moment ($M_0 = \sigma_Y t_s D^2$) and the curvature is normalized by the value of characteristic value $\kappa_I = t_s/D^2$. In the same Figure, the corresponding predictions from the J_2-flow theory are also shown. The prebuckling paths obtained from the 2 models are quite close, but the associative model fails to predict correct bifurcation. More specifically, the bifurcation predicted by the associative flow model occurs at a very late stage denoted by (↓) and does not correspond to wrinkled shape observed experimentally.

Failure of the cylinder occurs because of wrinkle localization (Figure 10); using an initially wrinkled model in the form of the shape of Figure 9 with a wrinkle amplitude equal to $\omega_{0,max}/t_s = 10^{-3}$ (consistent with reported

experimental measurements) and imposing a very small preference in the wrinkle of the middle section, the cylinder exhibits structural instability in the form of a localized buckled pattern. The corresponding moment-curvature curve matches very well the experimental curve. The above results are consistent with the observations reported in the corresponding experiments (Kyriakides and Ju, 1992).

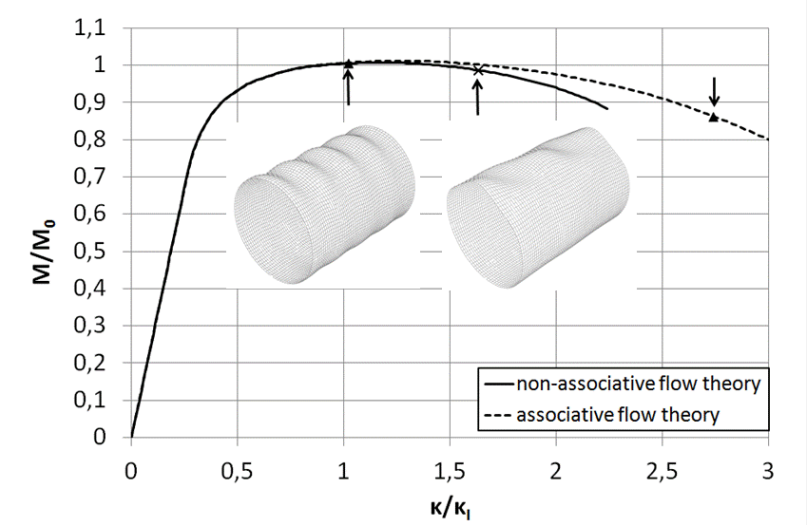

Figure 9: Moment-curvature diagram of tube with D/t_s =35.7.

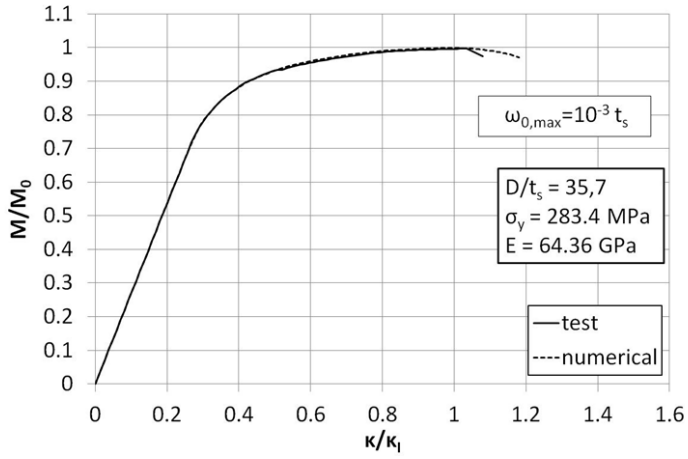

(a)

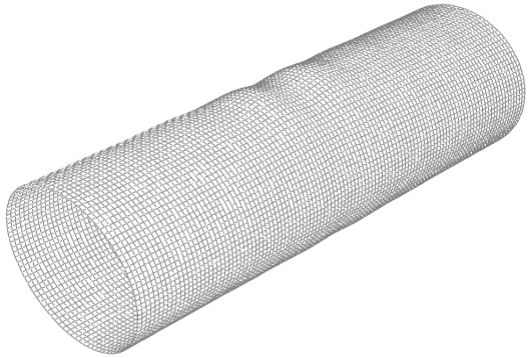

(b)

Figure 10: (a) Comparison of test results (Kyriakides and Ju, 1992) with present numerical predictions; (b) Deformed configuration of a bent shell with localized wrinkling (D/t_s =35.7).

7 CONCLUSIONS

A large-strain J_2 non-associative plasticity model has been developed for nonlinear analysis of cylindrical shells. The model maintains the basic formulation and implementation features of the standard J_2-flow theory, but contains the necessary enhancements for accurate shell buckling predictions, without any additional parameters required by corner or pseudo-corner theories. The model is consistent with shell theory requirements (zero stress normal to the shell laminae), it is numerically integrated through a robust Euler-backward substitution scheme. An alternative Euler-forward scheme is also presented. An enhanced large strain version of the model is also presented, based on an additive decomposition of the rate-of-deformation tensor. This allows the direct application of the above robust integration schemes in large-strain analysis through a polar decomposition of the deformation gradient and appropriate rotation of the stress and strain tensors, while accounting for zero stress normal to shell laminae. The non-associative constitutive model is implemented within a special-purpose finite element formulation, which uses a three-node "tube element". Bifurcation buckling in the inelastic range is detected along the equilibrium path through an implementation of the "comparison solid" concept. Special emphasis is paid on the continuity of plastic flow, to overcome numerical problems of convergence. Numerical results are in excellent agreement with available experimental data and analytical predictions, and demonstrate that the present methodology is capable of describing accurately and efficiently buckling and post-buckling behavior of rather think-walled cylindrical shells in the inelastic range. In addition, the comparison with test data demonstrates the superiority of this non-associative model with respect to the classical associative J_2–plasticity model in predicting shell buckling in the inelastic range.

ACKNOWLEDGEMENT

Financial support for this work has been provided from the Research Fund for Coal and Steel of the European Commission, within COMBITUBE project: "Bending Resistance of Steel Tubes in Combiwalls", Grant No RFSR-CT-2011-00034.

REFERENCES

Aravas, N., 1987. *On the numerical integration of a class of pressure dependent plasticity models*, International Journal for Numerical Methods in Engineering, Vol. 24, pp. 1395-1416

Argyris, J.H., Papadrakakis, M., Karapitta, L., 2002. *Elasto-plastic analysis of shells with the triangular element TRIC*, Computer Methods in Applied Mechanics and Engineering, Vol. 191, pp. 3613–3636.

Bardi, F.C., Kyriakides, S., 2006. *Plastic buckling of circular tubes under axial compression-part I: Experiments*, International Journal of Mechanical Sciences, Vol. 48, pp. 830-841.

Bardi, F.C., Kyriakides, S., Yun, H. D., 2006. *Plastic buckling of circular tubes under axial compression-part II: Analysis*, International Journal of Mechanical Sciences, Vol. 48, pp. 842-854.

Batterman, S. C., 1965. *Plastic buckling of axially compressed cylindrical shells*, AIAA Journal, 3, pp. 316-325.

Brush D.O., Almroth, B.O., 1975. *Buckling of bars, plates and shells*, McGraw Hill, New York, NY.

Christoffersen, J. and Hutchinson, J.W., 1979. *A class of phenomenological corner theories of plasticity*, J. Mech. Phys. Solids 27, pp. 465–487.

Crisfield, M.A., 1983. *An arc-length method including line searches and accelerations*, International Journal for Numerical Methods in Engineering, 19, pp. 1269-1289.

Dvorkin, E. D., Pantuso, D., Repetto, E. A., 1995. *A formulation of the MITC4 shell element for finite strain elasto-plastic analysis*, Computer Methods in Applied Mechanics and Engineering, Vol. 125, pp. 17-40.

Franca, L. P., 1989. *Algorithm to compute the square root of a 3x3 positive definite matrix*, Computers and Mathematics with Applications, 18 pp. 459-466.

Gellin, S., 1979. *Effect of an axisymmetric imperfection on the plastic buckling of an axially compressed cylindrical shell*, ASME J. Appl. Mech. 46, pp. 125–131.

Houliara, S., Karamanos, S.A., 2006. *Buckling and post-buckling of pressurized thin-walled elastic tubes under in-plane bending*, International Journal of Nonlinear Mechanics, 41, 4, pp. 491-511.

Houliara, S., Karamanos, S.A., 2010. *Stability of long transversely-isotropic elastic cylindrical shells under bending*, International Journal of Solids and Structures, Vol. 47, No. 1, pp. 10-24.

Hughes, T.J.R. and Shakib, F., 1986, *Pseudo-corner theory: A simple enhancement of J_2-flow theory for applications involving non-proportional damping*, Eng. Comput. Vol.3, pp.116-120.

Hutchinson, J.W., 1974. *Plastic buckling*, Advances n Applied Mechanics, Vol. 14, pp. 67-144.

Ju, G.T., Kyriakides, S., 1992. *Bifurcation and localization instabilities in cylindrical shells under bending II: predictions*, International Journal of Solids and Structures, Vol. 29, pp. 1143-1171.

Karamanos, S. A., 2002. *Bending instabilities of elastic tubes*, International Journal of Solids and Structures, 39, 8, pp. 2059-2085.

Karamanos, S.A., Tassoulas, J.L., 1996. *Tubular members I: stability analysis and preliminary results*, Journal of Engineering Mechanics, ASCE, 122, 1, pp. 64-71.

Koiter, W. T., 1963. *The effect of axisymmetric imperfections on the buckling of cylindrical shells under axial compression*, Koninkl. Nederl. Akademie van Wetenschappen, Amsterdam, Ser. B, Vol. 66, No. 5.

Kuwabara, T., Kuroda, M., Tvergaard, V. and Nomura K., 2000. *Use of abrupt strain path change for determining subsequent yield surface: experimental study with metal sheets*, *Acta Mater.* 48, pp. 2071–2079.

Kyriakides, S., Ju, G. T., 1992. *Bifurcation and localization instabilities in cylindrical Shells under bending I: Experiments*, *International Journal of Solids and Structures*, Vol. 29, pp. 1117-1142.

Lee, L. N. H., 1962. *Inelastic buckling of initially imperfect cylindrical shells subjected to axial compression*, Journal of Aerospace Science 29, pp. 87–95.

Malvern, L.E., 1969, *Introduction to the Mechanics of a Continuous Medium*, Prentice-Hall, Englewood Cliffs, NJ.

Mikkelsen, L.P., 1995. *Elastic−viscoplastic buckling of circular cylindrical shells under axial compression*, Eur. J. Mech. A/Solids 14, pp. 901–920.

Nagtegaal, J. C., 1982. *On the Implementation of Inelastic Constitutive equations with Special Reference to Large Deformation Problems*, Comp. Methods Appl. Mech. & Engrg., Vol. 33, pp. 469-484.

Neale, K.W., 1981. *Phenomenological constitutive laws in finite plasticity*, Solid Mechanics Archives 6, 79.

Needleman, A., 1982. *Finite elements for finite strain plasticity problems*, Plasticity of Metals at Finite Strain: Theory, Experiment and Computation, edited by E.H. Lee and R.L. Mallet, Rensselaer Polytechnic Institute, Troy, New York, pp. 387-436.

Paraskevopoulos, E., Talaslidis, D., 2006. *Reduction of excessive energy in the four-noded membrane quadrilateral element. Part II: Near incompressibility and J_2 plasticity*, Computer Methods in Applied Mechanics and Engineering, Vol. 196, pp. 356-370.

Pappa, P., 2015. *Numerical Simulation of Inelastic Shell Buckling and Post-Buckling Behavior*, Ph.D. Dissertation, Department of Mechanical Engineering, University of Thessaly, Greece.

Peek, R., 2000. *An incrementally continuous deformation theory of plasticity with unloading*, International Journal of Solids and Structures, Vol. 37, No 36, pp. 5009-5032.

Simo, J.C., 1987, *A J_2-flow theory exhibiting a corner-like effect and suitable for large-scale computation*, Computer Methods in Applied Mechanics and Engineering, Vol. 62, pp.169-94.

Simo, J. C. and Hughes, T. J. R., 1998. *Computational Inelasticity*, Springer, New York.

Ting, T. C. T., 1985. *Determination of $\mathbf{C}^{1/2}$, $\mathbf{C}^{-1/2}$ and more general isotropic tensor functions of $\mathbf{C}$*. J. Elasticity, 15(3):319–323.

Tvergaard, V., 1983. *Plastic buckling of axially compressed circular cylindrical shells*, Thin−Walled Structures 1, pp. 139–163.

Appendix I – Newton's method for integrating the constitutive model

Equations (27), (29), (33), (32) or (27), (37), (38), (32) are solved using the Newton method. The unknowns $\Delta\varepsilon_q$ and $\Delta\varepsilon_{33}$ are chosen as the primary unknowns considering that equations (32)and (33) or (32) and (38) are the basic equations. Denoting as $\delta\left(\Delta\varepsilon_q\right)$ and $\delta\left(\Delta\varepsilon_{33}\right)$ the corrections of c and $\Delta\varepsilon_{33}$, the Newton equations become:

$$\begin{bmatrix} A_{11} & A_{12} \\ A_{21} & A_{22} \end{bmatrix} \begin{bmatrix} \delta\left(\Delta\varepsilon_q\right) \\ \delta\left(\Delta\varepsilon_{33}\right) \end{bmatrix} = \begin{bmatrix} b_1 \\ b_2 \end{bmatrix} \tag{I-1}$$

For the backward-Euler integration scheme, the constants A_{ij} and b_i are given in the following expressions:

$$A_{11} = \frac{\partial f_1}{\partial \Delta\varepsilon_q} = \frac{\partial q}{\partial \Delta\varepsilon_q} - \frac{\partial k}{\partial \Delta\varepsilon_q} = \frac{\partial q}{\partial \Delta\varepsilon_q} - H \tag{I-2}$$

$$A_{12} = \frac{\partial f_1}{\partial \Delta\varepsilon_{33}} = \frac{\partial q}{\partial \Delta\varepsilon_{33}} - \frac{\partial k}{\partial \Delta\varepsilon_{33}} = \frac{\partial q}{\partial \Delta\varepsilon_{33}} \tag{I-3}$$

$$A_{21} = \frac{\partial f_2}{\partial \Delta\varepsilon_q} = \frac{3G}{h_{n+1}^2} s_n^{33} + p_{n+1}\, g^{33} \left(-\frac{3G h'_{1|n+1}}{h_{n+1}^2} + \frac{\left(3G\Delta\varepsilon_q H'_{n+1} + 3G H_{n+1}\right) q_{n+1} h_{1|n+1} - 3G\Delta\varepsilon_q H_{n+1} \left(\dfrac{\partial q}{\partial \Delta\varepsilon_q} h_{1|n+1} + q_{n+1} h'_{1|n+1} \right)}{q_{n+1}^2 h_{1|n+1}^2} \right) \tag{I-4}$$

$$A_{22}=\frac{\partial f_2}{\partial\Delta\varepsilon_{33}}=\left(1+\frac{3G}{h_{n+1}}+\frac{3G\,\Delta\varepsilon_q\,H_{n+1}}{q_{n+1}h_{1|n+1}}\right)\left(-Kg^{33}\right)g^{33} - \frac{3G\,\Delta\varepsilon_q\,H_{n+1}h_{1|n+1}}{q_{n+1}^2h_{1|n+1}^2}\frac{\partial q}{\partial\Delta\varepsilon_{33}}\,p_{n+1}\,g^{33}-\frac{4}{3}Gg^{33}g^{33} \tag{I-5}$$

and

$$b_1=-q_{n+1}\left(\Delta\varepsilon_q,\Delta\varepsilon_{33}\right)+k\left(\varepsilon_{q|n}+\Delta\varepsilon_q\right) \tag{I-6}$$

$$b_2=-\left(1+\frac{3G}{h_{n+1}}+\frac{3G\,\Delta\varepsilon_q\,H_{n+1}}{qh_{1|n+1}}\right)p_{n+1}\,g^{33}+\left(\overline{s}^{(e)^{33}}+\frac{4G}{3}\Delta\varepsilon_{33}\,g^{33}\,g^{33}+\frac{3G}{h_{n+1}}s^{33}\right) \tag{I-7}$$

where

$$\frac{\partial q\left(\Delta\varepsilon_q,\Delta\varepsilon_{33}\right)}{\partial\Delta\varepsilon_q}=\left(\frac{3Gh'_{1|n+1}\,h_{n+1}^{-2}}{1+3G\,h_{n+1}^{-1}}\right)q_{n+1}+\left(\frac{1}{1+3G\,h_{n+1}^{-1}}\right) \left\{\frac{\left(3G\,\Delta\varepsilon_q\,H'_{n+1}+3G\,H_{n+1}\right)}{h_{1|n+1}}+\frac{3G\,\Delta\varepsilon_q\,H_{n+1}h'_{1|n+1}}{h_{1|n+1}^2} + \frac{-9G^2h'_{1|n+1}\,h_{n+1}^{-3}\,q_n^2-3Gh'_{1|n+1}\,h_{n+1}^{-2}\,Q^2-9G^2\,\Delta\varepsilon_{33}\,h'_{1|n+1}\,h_{n+1}^{-2}\,s_n^{33}}{\left(1+3G\,h_{n+1}^{-1}\right)q_{n+1}+3G\,\Delta\varepsilon_q\,H_{n+1}h_{1|n+1}^{-1}}\right\} \tag{I-8}$$

$$\frac{\partial q\left(\Delta\varepsilon_q,\Delta\varepsilon_{33}\right)}{\partial\Delta\varepsilon_{33}}=\left(\frac{1}{1+3G\,h_{n+1}^{-1}}\right)\left(\frac{4G^2\,\Delta\varepsilon_{33}\,g^{33}\,g^{33}+3G\left(\overline{s}^{(e)^{33}}+3G\,h_{n+1}^{-1}\,s_n^{33}\right)}{\left(1+3G\,h_{n+1}^{-1}\right)q_{n+1}+3G\,\Delta\varepsilon_q\,H_{n+1}h_{1|n+1}^{-1}}\right) \tag{I-9}$$

For the forward-Euler integration scheme, the constants A_{ij} and b_i are given in the following expressions:

$$A_{11}=\frac{\partial f_1}{\partial\Delta\varepsilon_q}=\frac{\partial q}{\partial\Delta\varepsilon_q}-\frac{\partial k}{\partial\Delta\varepsilon_q}=\frac{\partial q}{\partial\Delta\varepsilon_q}-H \tag{I-10}$$

$$A_{12}=\frac{\partial f_1}{\partial\Delta\varepsilon_{33}}=\frac{\partial q}{\partial\Delta\varepsilon_{33}}-\frac{\partial k}{\partial\Delta\varepsilon_{33}}=\frac{\partial q}{\partial\Delta\varepsilon_{33}} \tag{I-11}$$

$$A_{21}=\frac{\partial f_2}{\partial\Delta\varepsilon_q}=-\frac{3G\,H_{n+1}}{q_nh_{1|n}}s_n^{33} \tag{I-12}$$

$$A_{22}=\frac{\partial f_2}{\partial\Delta\varepsilon_{33}}=-\left(1+\frac{3G}{h_n}\right)\left(-Kg^{33}\right)g^{33}+\frac{4}{3}Gg^{33}g^{33} \tag{I-13}$$

and

$$b_1=-q_{n+1}\left(\Delta\varepsilon_q,\Delta\varepsilon_{33}\right)+k\left(\varepsilon_{q|n}+\Delta\varepsilon_q\right) \tag{I-14}$$

$$b_2=-\left(1+\frac{3G}{h_n}+\frac{3G\,\Delta\varepsilon_q\,H_n}{qh_{1|n}}\right)p_{n+1}\,g^{33}+\left(\overline{s}^{(e)^{33}}+\frac{4G}{3}\Delta\varepsilon_{33}\,g^{33}\,g^{33}+\frac{3G}{h_n}s^{33}\right) \tag{I-15}$$

where

$$\frac{\partial q\left(\Delta\varepsilon_q,\Delta\varepsilon_{33}\right)}{\partial\Delta\varepsilon_q}=\left(-\frac{H_n\,q_n^{-1}h_{1|n+1}^{-1}}{\left(1+3G\,h_n^{-1}\right)^2 q_{n+1}}\right)\left(9G^2\left(\frac{1}{h_n}-\frac{\Delta\varepsilon_q\,H_n}{q_n h_{1|n}}\right)q_n^2 + 3G^2\,Q^2+9G^2\,\Delta\varepsilon_{33}\,s_n^{33}\right) \tag{I-16}$$

$$\frac{\partial q\left(\Delta\varepsilon_q,\Delta\varepsilon_{33}\right)}{\partial\Delta\varepsilon_{33}}=\left(\frac{1}{1+3G\,h_n^{-1}}\right)\left(\frac{4G^2\,\Delta\varepsilon_{33}\,g^{33}\,g^{33}+3G\,\overline{s}^{(e)^{33}}}{\left(1+3G\,h_n^{-1}\right)q_{n+1}} + \frac{9G^2\left(h_n^{-1}+H_n\,\Delta\varepsilon_q\,q_n^{-1}\,h_{1|n}^{-1}\right)s_n^{33}}{\left(1+3G\,h_n^{-1}\right)q_{n+1}}\right) \tag{I-17}$$

Appendix II - Algorithm for polar decomposition

This algorithm computes the squares of the principal stretches λ_i^2, $(i=1,2,3)$ (the eigenvalues of $\mathbf{C}$) by solving (in closed form) the characteristic polynomial. The algorithm has been introduced by Franca (1989), it is described in the book of Simo and Hughes (1998) and is adapted herein for the case of curvilinear coordinates. The covariant base vector and the contravariant (reciprocal) base vector in the beginning of the step $\mathbf{G}_i$, $\mathbf{G}^j$, the covariant base vector and the contravariant base vector in the current configuration $\mathbf{g}_i$, $\mathbf{g}^j$ respectively, are given. Let a_i, $(i=1,2,3)$ be the principal invariants of $\mathbf{U}$ defined as

$$\begin{aligned} a_1 &= g_{ij}G^{ij} \\ a_2 &= \frac{1}{2}\left[\left(g_{ij}G^{ij}\right)^2 - a_{ij}G^{ij}\right] \\ a_3 &= \det\left(g_{ik}\right) \end{aligned} \tag{II-1}$$

and

$$\begin{aligned} b &= a_2-\frac{a_1^2}{3} \\ d &= -\frac{2}{27}a_1^3+a_1\frac{a_2}{3}-a_3 \end{aligned} \tag{II-2}$$

where

$$a_{ij}=g_{ik}g_{jl}G^{kl} \tag{II-3}$$

If $b=0$ ($b<tol$)

$$\lambda_1=\lambda_2=\lambda_3=\sqrt{\frac{a_1}{3}} \tag{II-4}$$

else

$$\begin{aligned} m &= 2\sqrt{\frac{-b}{3}} \\ n &= \frac{3d}{mb} \\ aux &= 1-n^2 \end{aligned} \tag{II-5}$$

If $aux<0$ then

$$\begin{aligned} &if\ \ n>1 \Rightarrow t=0 \\ &if\ \ n<1 \Rightarrow t=\frac{\pi}{3} \end{aligned} \tag{II-6}$$

else

$$t=\frac{1}{3}arctan\left(\frac{\sqrt{aux}}{n}\right) \tag{II-7}$$

end if

$$x_i = m\cos\left[t+\frac{2(i-1)\pi}{3}\right],\ i=1,2,3 \tag{II-8}$$

and

$$\begin{aligned} &\lambda_i^2 = x_i + \frac{a_1}{3} \\ &\lambda_i = \sqrt{\lambda_i^2} \end{aligned} \tag{II-9}$$

end if

Compute the invariants of $\mathbf{U}$

$$\begin{aligned} &i_1 = \lambda_1+\lambda_2+\lambda_3 \\ &i_2 = \lambda_1\lambda_2+\lambda_2\lambda_3+\lambda_3\lambda_1 \\ &i_3 = \lambda_1\lambda_2\lambda_3 \end{aligned} \tag{II-10}$$

Furthermore, the coefficients A_i, B_i (i=1,2,3) in the expressions (73) and (76) for $\mathbf{U}$, $\mathbf{U}^{-1}$ are defined as

$$\begin{aligned} &A_1 = -\frac{1}{D} \\ &A_2 = \frac{\left(i_1^2-i_2\right)}{D} \\ &A_3 = \frac{i_1 i_3}{D} \end{aligned} \tag{II-11}$$

and

$$\begin{aligned} &B_1 = \frac{1}{i_3} \\ &B_2 = \frac{-i_1}{i_3} \\ &B_3 = \frac{i_2}{i_3} \end{aligned} \tag{II-12}$$

where $D = i_1 i_2 - i_3$.